

RBFs methods for null control problems of the Stokes system with Dirichlet and Navier–slip boundary conditions.

Pedro González–Casanova*, Louis Breton† and Cristhian Montoya‡

Abstract

The purpose of this article is to introduce radial basis function, (RBFs), methods for solving null control problems for the Stokes system with few internal scalar controls and Dirichlet or Navier–slip boundary conditions. To the best of our knowledge, it has not been reported in the literature any numerical approximation through RBFs to solve the direct Stokes problem with Navier–slip boundary conditions. In this paper we fill this gap to show its application for solving the null control problem for the Stokes system. To achieve this goal, we introduce two radial basis function solvers, one global and the other local, to discretized the primal and adjoint systems related to the control problem. Both techniques are based on divergence-free global RBFs. Stability analysis for these methods is performed in terms of the spectral radius of the corresponding Gram matrices. By using a conjugate gradient algorithm, adapted to the radial basis function setting, the control problem is solved. Several test problems in two dimensions are numerically solved by these RBFs methods to test their feasibility. The solutions to these problems are also obtained by finite elements techniques, (FE), to compare their relative performance.

Key Words: Stokes system, null controllability, Navier–slip boundary conditions, radial basis functions, conjugate gradient method, local Hermite interpolation method.

1 Introduction

The main goal of this article is to introduce radial basis function, (RBFs), methods to solve null control problems for the Stokes system with few internal scalar controls and Dirichlet or Navier–slip boundary conditions. In order to solve this problem, we first present fast and efficient radial basis functions (RBFs) algorithms for the Stokes equations with Dirichlet or Navier–slip boundary conditions, and to solve from a numerical point of view the null control problem associated to the Stokes system with such boundary conditions. The control function is given as an external source acting over a subdomain and having few scalar controls, for example, the control function can be $\mathbf{v} = (v_1, 0)$, where v_1 is a scalar field supported in a small subdomain. First, we mention some recent discretization schemes linked to the direct Stokes problem with Dirichlet conditions. The notion of the null control problem for the Stokes system will be mentioned later on.

Stationary and evolutionary Stokes equations have been recently solved using analytically divergence-free and curl-free approximation spaces, [Wen09] and [FSW16]. These schemes involve matrix-valued, positive definite kernels, as they have been introduced in [AB91] and [NW94].

¹Instituto de Matemáticas, Universidad Nacional Autónoma de México, México. casanova@matem.unam.mx

²Facultad de Ciencias, Universidad Nacional Autónoma de México, México. louis.breton@ciencias.unam.mx

³Departamento de Matemática, Universidad Técnica Federico Santa María, Casilla 110-V, Valparaíso, Chile. cristhian.montoya@usm.cl

In [Wen09], using the well known fact that the vector field \mathbf{u} has a vector potential \mathbf{w} , i.e., that $\mathbf{u} = \nabla \times \mathbf{w}$, the author define the potential as the curl of a scalar compact support radial basis function ψ , i.e., $\mathbf{w} = \Delta \times \psi$. The field \mathbf{u} is then approximated by a linear combination of the divergency-free matrix-valued kernel $\Phi_{Div} = \nabla \times \Delta \times \psi = \{-\Delta I + \nabla \nabla^T\} \psi(\mathbf{x})$, where Δ is the Laplacian and I the identity matrix. A basic element in this approach, is that the author utilizes a vector composed by the velocity and the pressure, i.e., the vector $(\mathbf{u}, p) \in \mathbb{R}^{d+1}$. Thus, by forming an Ansatz build from a combination of a divergency free RBF kernel Φ_{Div} and a scalar RBF kernel ψ , he is able to discretize the stationary Stokes problem such that incompressibility is analytically satisfied. Boundary conditions are incorporated to the discrete scheme, which is proved to be invertible. *It is important to note that both the velocity and the pressure are coupled in the algebraic system of this approach.*

Within the same spirit, in [FSW16], they built both a divergency free Φ_{Div} and a rotational free $\Psi_{Rot} = -\nabla \nabla^T \psi(\mathbf{x})$ matrix-valued kernels. Two major differences with respect to the first work, is that in [FSW16], the radial basis function ψ is now global and that they solve the evolutionary instead the stationary Stokes problem. In fact, based in the Leray projection, which is based in the Hodge decomposition theorem, they first decouple the Stokes equation into a forced diffusion-type equation for \mathbf{u} and then using the ortogonal complement of the Leray projector they obtain an auxiliary equation for the gradient of the pressure in terms of the velocity \mathbf{u} . These two equations are then discretized, for the space variable, by collocation using the RBFs kernel Φ_{Div} for the velocity and ψ for the pressure. Using the method of lines with a proper time integrator they solve the evolutionary Stokes problem.

We stress that in [FSW16], unlike the current standard Leray-type projection methods [BCM01], the method proposed by the authors allows to build both tangential and normal boundary conditions into the discrete approximation to the Leray projection. This is in the spirit of RBFs global Hermite or symmetric methods for the solution of scalar PDEs, [Fas07]. However, we emphasize that this scheme imposes non-slip boundary conditions. This is a consequence of the fact that the Leray projector applied to the stationary Stokes problem, eliminates the pressure from corresponding velocity equation, which in turn means that we cannot impose slip boundary conditions using the decouple procedure as it is currently proposed by Fuselier, [FSW16].

A first limitation of the method given in [FSW16] is that it incurs two dimension-dependent costs: an initialization cost of $O(N^3)$, and a cost of $O(N^2)$ per time-step, where N is the total number of nodes. This is a consequence of the use of global RBFs to approximate the Leray projector. A second limitation, which is well known for RBF global methods, is that the condition number of the Gram matrix increases very fast as the number of nodes grows, thus limiting the size of the problems that can be solved.

We note that the method introduced by Kein and Wendland, [KW16], is based upon the Leray projection, which converts the Stokes equation into a vector-valued heat equation. As mention above, our approach, heavily relies on Wendland method that incorporates the pressure into the solution. However, a difference is that we use global instead compact support RBFs to build the incompressible vector. Also in our approach we do not use the Leray projection to transform the system into a vector-valued heat equation. Finally we incorporate Navier–slip boundary conditions into the direct solver of the stokes problem.

The approach to solve the direct Stokes problem that we introduce in this paper has two proposes. First we use Wendland formulation [Wen09], for global RBFs, to solve the stationary and evolutionary Stokes problems for the velocity and pressure simultaneously. Thus, we can perform the discretization for Navier–slip boundary conditions, and second we aim to suppress the former limitations of Fuselier algorithm. Specifically, we use a RBFs Local Hermite Method instead the global Hermite or symmetric collocation technique. By using extended precession it possible to solve problems having a large number of data. This is possible, whenever the value of the fill distance and shape parameter have values such that the condition number of the

local matrices, in extended precision, are numerically well posed. Also the numerical complexity of the algorithm, (CPU time), is reduced with respect to global methods. It is worth noting that, although here we aim to investigate the extended precision approach, several alternatives to the ill-conditioned problem of RBFs collocation methods have been recently formulated, see for example [LSW17, FLP13, FF15] and references therein for a comprehensive review on this subject. We also recall that in a different context, namely for interpolation of vector fields, both global techniques and LHI methods have been investigated by one of the authors, (see [CGCG⁺13], [CGCGM18]).

Once the direct methods are formulated, our approximation strategy to solve the null control problem for the Stokes system is based in applying the conjugate gradient method (CGM) for PDE's, supported on the classical formulation for control problems under the form of appropriate convex quadratic optimization problems [GL94, GLH08]. In this work, numerical experiments are carried out in two dimensions using distributed controls with either all scalar components or few scalar controls and taking into account the two types of boundary conditions, Dirichlet and Navier–slip. Moreover, we use finite elements to obtain numerical solutions of these problems and compare its performance against the RBF results.

Following in the context of the null control problem, the numerical setting for the RBF algorithm has thus two parts:

- A fast and efficient RBFs solver for the evolutionary Stokes problems.
- A splitting iterative algorithm, namely the conjugate method (CGM), to solve the coupled system of equations (optimal system).

It is worth mentioning that only a few articles have appeared in radial basis function methods in control theory. Up to our knowledge, only two works on optimal control by RBF techniques has been reported in this field, [Pea13] and [GZ18].

The paper is organized as follows. In Section 2 we give the continuous description of the null control problem. Section 3 we recall some algorithmic elements of the LHI method. The divergence free global method and stability results are developed in Section 4. In Section 5, we introduce a RBF–LHI approach for solving the Stokes system. Finally, in Section 6 we conclude the paper by applying these RBFs methods to the null controllability problem with few scalar controls and either Dirichlet or Navier–slip conditions. Conclusions and final remarks are also included.

2 Problem formulation

In this section we introduce the notation and the continuous setting of the Stokes control problem that will be numerically solved in this article.

Let us first introduce some notation. Let Ω be a nonempty bounded connected open subset of \mathbb{R}^d ($d = 2$ or $d = 3$) of class C^∞ . Let $T > 0$ and let $\omega \subset \Omega$ be a (small) nonempty open subset which is the control domain. Let further $Q := \Omega \times (0, T)$, $\Sigma := \partial\Omega \times (0, T)$ and by $\boldsymbol{\nu}(x)$ the outward unit normal vector to Ω at the point $x \in \partial\Omega$.

Moreover, let

$$H := \{\mathbf{u} \in L^2(\Omega)^d : \nabla \cdot \mathbf{u} = 0 \text{ in } \Omega, \mathbf{u} \cdot \boldsymbol{\nu} = 0 \text{ on } \partial\Omega\}$$

and

$$V := \{\mathbf{u} \in H_0^1(\Omega)^d : \nabla \cdot \mathbf{u} = 0 \text{ in } \Omega\}.$$

The continuous null control problem for the Stokes system with either Dirichlet or Navier–slip boundary conditions, that we are interested in, is defined as follows:

Given an initial data y_0 , we are looking for a control function $\mathbf{v} = \mathbf{v}(x, t)$ acting in $\omega \times (0, T)$ with $\text{supp } \mathbf{v} \subset \omega \times (0, T)$ such that the solution of the problem

$$\begin{cases} \mathbf{y}_t - \mu \nabla \cdot (D\mathbf{y}) + \nabla p = \mathbf{v} 1_\omega & \text{in } Q, \\ \nabla \cdot \mathbf{y} = 0 & \text{in } Q, \\ +\text{BC} & \text{on } \Sigma, \\ \mathbf{y}(\cdot, 0) = \mathbf{y}_0(\cdot) & \text{in } \Omega, \end{cases} \quad (2.1)$$

satisfies

$$\mathbf{y}(\cdot, T) = 0 \quad \text{in } \Omega. \quad (2.2)$$

In (2.1), D denotes the symmetrized gradient of \mathbf{y} , $\mu > 0$ is the viscosity coefficient and p is the pressure .

We focus our work in two types of boundary conditions (BC) on Σ , namely:

$$\underbrace{\mathbf{y} = 0}_{(a) \text{ Dirichlet}} \quad \text{or} \quad \underbrace{\mathbf{y} \cdot \boldsymbol{\nu} = 0, \quad (\sigma(\mathbf{y}, p) \cdot \boldsymbol{\nu})_{tg} = 0}_{(b) \text{ Navier–slip}}, \quad (2.3)$$

where $\sigma(\mathbf{y}, p) := -pId + 2\mu D\mathbf{y}$ is the stress tensor and tg stands for the tangential component of the corresponding vector field, i.e.,

$$\mathbf{y}_{tg} = \mathbf{y} - (\mathbf{y} \cdot \boldsymbol{\nu})\boldsymbol{\nu}.$$

From a Physical point of view, Navier–slip boundary condition arises from the interaction between wall and fluid and when the temperature is high. These behavior involves a movement on the boundary (slip), losing energy, which do not penetrate the boundary (impermeable boundary), among other factors. The use of these slip conditions allow to describe phenomena observed in nature and remove un–physical singularities, see for instance [Ceb12], [HW09] and references therein for more details. Now, from a mathematical point of view, such boundary conditions say that the tangential component of the stress tensor is proportionality to the tangential component of the velocity [Nav23]:

$$\mathbf{y} \cdot \boldsymbol{\nu} = 0, \quad (\sigma(\mathbf{y}, p) \cdot \boldsymbol{\nu})_{tg} + k\mathbf{y}_{tg} = 0,$$

where k is a function that measures the local viscous coupling fluid–solid. We highlight that this proportionality factor can depend on the velocity as well as on the pressure, which complicate both the theoretical analysis and numerical solutions. In our numerical experiments we only deal the case (2.3)–(b) and invite to interested reader to see [Ceb12, Nav23] for a complete discussion on this subject.

We now characterize the control problem in terms of the optimal or minimum value of a quadratic convex functional in $(L^2(Q))^2$ in the sense of [GMO17].

Namely, for $\mathbf{y}_0 \in H$, we aim to obtain the control \mathbf{v} with one vanishing component (j th component, $j \in \{1, 2\}$) such that it minimizes the functional J defined by

$$J(\mathbf{v}) := \frac{1}{2} \iint_{\omega \times (0, T)} |\mathbf{v}|^2 dx dt + \frac{1}{2c_1} \|\mathbf{y}(\cdot, T)\|_{L^2(\Omega)}^2 dx + \frac{1}{2c_2} \iint_{\omega \times (0, T)} |v_j|^2 dx dt, \quad (2.4)$$

where \mathbf{y} is solution of the Stokes system (2.1), c_1, c_2 are arbitrary positive numbers associated respectively to the final condition $\mathbf{y}(\cdot, T) = 0$ and control function \mathbf{v} .

As it is well known, this problem can be restated in terms of the Lagrangian formulation. Let $\mathcal{L} : [H_0^1(\Omega)^2]^2 \times [L_0^2(\Omega)]^2 \times L^2(Q)^2 \rightarrow \mathbb{R}$ defined by:

$$\begin{aligned} \mathcal{L}(\mathbf{y}, \mathbf{w}, q, p, \mathbf{v}) := & \frac{1}{2} \iint_{\omega \times (0, T)} |\mathbf{v}|^2 dx dt + \frac{1}{2c_1} \|\mathbf{y}(\cdot, T)\|_{L^2(\Omega)}^2 dx + \frac{1}{2c_2} \iint_{\omega \times (0, T)} |v_j|^2 dx dt \\ & + \iint_Q \mathbf{y}_t \cdot \mathbf{w} - \mu \nabla \cdot (D\mathbf{y}) \cdot \mathbf{w} - \operatorname{div}(\mathbf{w})p - \operatorname{div}(\mathbf{w})q dx dt \\ & - \iint_{\omega \times (0, T)} \mathbf{v} \cdot \mathbf{w} dx dt + \int_{\Omega} (\mathbf{y}(\cdot, 0) - \mathbf{y}_0) \cdot \mathbf{w}(\cdot, 0) dx, \end{aligned} \quad (2.5)$$

where \mathbf{w} is the Lagrange multiplier. The optimal value of the control \mathbf{v} can be obtained in the following way. It is easy to verify that the Fréchet derivate of J with respect to \mathbf{v} is:

$$\frac{\partial J}{\partial \mathbf{v}}(\mathbf{v}) = v_i - w_i \text{ if } i \neq j \quad \text{and} \quad \frac{\partial J}{\partial \mathbf{v}}(\mathbf{v}) = \frac{1}{2c_2} v_j - w_j, \quad \text{in } \omega \times (0, T), \quad (2.6)$$

where $\mathbf{w} \in V$ is the solution of the adjoint system of (2.1):

$$\begin{cases} -\mathbf{w}_t - \mu \nabla \cdot D\mathbf{w} + \nabla q = 0 & \text{in } Q, \\ \nabla \cdot \mathbf{w} = 0 & \text{in } Q, \\ +\text{BC} & \text{on } \Sigma, \\ \mathbf{w}(\cdot, T) = -\frac{1}{c_1} \mathbf{y}(\cdot, T) & \text{in } \Omega. \end{cases} \quad (2.7)$$

In [GMO17] the authors proved that for every $c_1 > 0$, $c_2 > 0$, there exists a unique minimal control \mathbf{v} associated to (2.4) which is characterized by the optimality system given by (2.1), (2.6), (2.7) with Dirichlet boundary conditions (2.3)–(a).

We stress that the Lagrangian formulation (2.5) is the continuous setting for the mixed FE formulation that will be used in the subsection of numerical results.

From an abstract point of view, the control theory for the Stokes system with internal controls has been studied intensively for the mathematical community. The interested reader can be see [FI99, FCGIP04, Cor96, Ima97, Gue06, CG13, CL14, GM18] and references therein for a complete description. Meanwhile, from a computational point of view, we only know the recent paper by Fernandez–Cara et. al, [FCMS17], whose numerical experiments are developed in two dimension for the heat, Stokes and Navier–Stokes with Dirichlet boundary conditions. The implemented methodology in [FCMS17] for the fluid equations is based in the so called Fursikov–Imanuvilov formulation [FI96] and Lagrangian approximation throughout mixed finite elements. Another approximation scheme to the null control problem is given in [FCLdM15] for a turbulence model and also using Dirichlet boundary conditions.

We close this section by pointing out that, as far as we know, it does not exists a numerical approximation through RBFs for the Stokes problem with Navier–slip boundary conditions. In the following sections we fill this gap and show its application for solving the null control problem for the Stokes system with few scalar controls.

3 Numerical method: notation and preliminary remarks

In what follows, and for the sake of completeness, we first briefly recall the scalar LHI method, introduced by Stevens, et al. [SPLM11]. (see [GZ18] for a similar notation). This scalar setting will be used later in this paper to formulate the generalized vectorial technique to solve the Stokes problem.

In the LHI scalar approach, we aim to obtain the RBF approximation of the analytic solution u of a linear steady partial differential well posed problem

$$\begin{cases} \mathcal{L}u(x) = f(x) & \text{in } \Omega, \\ \mathcal{B}u(x) = g(x) & \text{on } \partial\Omega, \end{cases} \quad (3.1)$$

where $\Omega \subset \mathbb{R}^d$ represents the spatial domain, the right-hand sides $f : \Omega \rightarrow \mathbb{R}$ and $g : \partial\Omega \rightarrow \mathbb{R}$

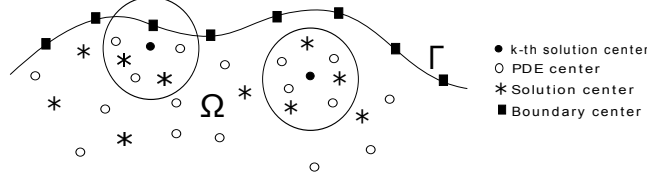


Figure 3.1: Centers and local subdomains for the LHI method

are given, \mathcal{L} and \mathcal{B} are linear partial differential operators in the domain Ω and on the contour $\partial\Omega$, which are locally approximated in the following way. First, let $\Omega_n \subset \bar{\Omega}$ be a set of n_t total number of scattered nodes. Consider now the following subsets of Ω_n . Let $\Omega_c \subset \Omega_n$ be a subset of n_c nodes called centers, see Figure 3.1.

Let now D^k be a disk, of variable radius, with center at the k^{th} node of Ω_c , (recall that Ω_c is the set of centers of the disks), and consider the set of $n^{(k)}$ fixed number of nodes $\Omega_n \cap D^k$, see again Figure 3.1. To perform the local discretization we introduce the following notation:

$$\begin{aligned} \Omega_{sc} &= \{x_1^{(k)}, \dots, x_{n_{sc}^k}\} \subset \Omega_c \text{ be a set of } n_{sc}^k \text{ nodes (called solution centers).} \\ \partial\Omega_{fc} &= \{x_{n_{sc}^k+1}^{(k)}, \dots, x_{n_{sc}^k+n_{fc}^k}\} \subset \partial\Omega \text{ the boundary nodes.} \\ \Omega_{pdec} &= \{x_{n_{sc}^k+n_{fc}^k+1}^{(k)}, \dots, x_{n_{sc}^k+n_{fc}^k+n_{pdec}^k}\} \subset \Omega \text{ is a set of interior nodes related } \mathcal{L}. \end{aligned}$$

By simplicity, we shall denote the node $x_1^{(k)}$ as the center of the disk D^k for each k . Then, every disk D^k define a local sub-system as follows:

$$\mathcal{L}u(x) = f(x) \quad x \in \Omega_{pdec}, \quad (3.2)$$

$$\mathcal{B}u(x) = g(x) \quad x \in \partial\Omega_{fc}, \quad (3.3)$$

$$u(x_i) = h_i \quad x_i \in \Omega_{sc}, \quad (3.4)$$

where h_i are the unknown values.

This procedure generates a set of local linear systems given by

$$A^{(k)}\beta^{(k)} = d^{(k)}, \quad (3.5)$$

which is obtained by substituting in (3.2)–(3.4) the following radial ansatz for the local domains displayed (in circles) in Figure 3.1

$$\hat{u}^{(k)}(x) = \sum_{j=1}^{n_{sc}^k} \beta_j^{(k)} \phi_j(r) + \sum_{j=n_{sc}^k+1}^{n_{sc}^k+n_{fc}^k} \beta_j^{(k)} \mathcal{B}^\xi \phi_j(r) + \sum_{j=n_{sc}^k+n_{fc}^k+1}^{n_{sc}^k+n_{fc}^k+n_{pdec}^k} \beta_j^{(k)} \mathcal{L}^\xi \phi_j(r) + p_k^m, \quad (3.6)$$

where k is the local system index, n_{sc}^k the number of solution centers in the local system, n_{pdec}^k denotes the number of PDE centers in the local system and n_{fc}^k is the number of boundary centers in the local system. Besides, $\mathcal{L}^\xi \phi_j(r) := \mathcal{L}\phi(\|x - \xi\|)|_{\xi=\xi_j}$, $\mathcal{B}^\xi \phi_j(r) := \mathcal{B}\phi(\|x - \xi\|)|_{\xi=\xi_j}$, being $\phi(r)$ the inverse multi-quadric and p_k^m a polynomial in \mathbb{R}^d of degree m , which is an element of the null space of (3.1). The momentum condition is also required in this step, see [SPLM11].

Thus, the local linear system (3.5) can be expressed in vectorial notation by defining $A^{(k)}$ (called Gram matrix) and the right hand vector $d^{(k)}$ as follows

$$A^{(k)} = \begin{bmatrix} \Phi_{ij} & \mathcal{B}^\xi[\Phi_{ij}] & \mathcal{L}^\xi[\Phi_{ij}] & P_{ij} \\ \mathcal{B}^x[\Phi_{ij}] & \mathcal{B}^x\mathcal{B}^\xi[\Phi_{ij}] & \mathcal{B}^x\mathcal{L}^\xi[\Phi_{ij}] & \mathcal{B}^x[P_{ij}] \\ \mathcal{L}^x[\Phi_{ij}] & \mathcal{L}^x\mathcal{B}^\xi[\Phi_{ij}] & \mathcal{L}^x\mathcal{L}^\xi[\Phi_{ij}] & \mathcal{L}^x[P_{ij}] \\ P_{ji} & \mathcal{B}^\xi[P_{ji}] & \mathcal{L}^\xi[P_{ji}] & 0 \end{bmatrix} \quad \text{and} \quad d^{(k)} = \begin{bmatrix} h_i \\ g_i \\ f_i \\ 0 \end{bmatrix},$$

which is well known to be invertible, see [Wen04]. Thus, we have that $\beta^{(k)} = (A^{(k)})^{-1}d^{(k)}$, and using (3.6), $\hat{u}^{(k)}(x)$ can be rewritten by

$$\hat{u}^{(k)}(x) = H(x)\beta^{(k)} = H(x)(A^{(k)})^{-1}d^{(k)} = W^{(k)}d^{(k)}, \quad (3.7)$$

where

$$H^{(k)}(x) = [\phi(\|x - \xi\|) \quad \mathcal{B}^\xi\phi(x - \xi) \quad \mathcal{L}^\xi\phi(\|x - \xi\|) \quad p^m(x)] \quad \text{and} \quad W^{(k)} := H(x)(A^{(k)})^{-1}.$$

$W^{(k)}$ is known as the vector of weights, [Wen04]. Now, if \mathcal{J} is an arbitrary differential operator given, we can compute its value at $\hat{u}^{(k)}$ by

$$\mathcal{J}\hat{u}^{(k)}(x) = \mathcal{J}H(x)(A^{(k)})^{-1}d^{(k)} = \mathcal{J}(W^{(k)})(x)d^{(k)}.$$

Let $u_c = [u(x_1^{(k)})]_{k=1}^{n_c^{(k)}}$ be the set of values of the exact solution at the centers of each disk D^k , which are unknown values (they belong to the vector $d^{(k)}$). In order to obtain these unknown values, we consider the following system of equations

$$h(x_1^{(k)}) = W_{\mathcal{J}}^{(k)}(x_1^{(k)})d^{(k)}, \quad k = 1, \dots, n_c, \quad (3.8)$$

where $W_{\mathcal{J}}^{(k)} = \mathcal{J}(W^{(k)})$ and (h, \mathcal{J}) is defined by (f, \mathcal{L}) .

We shall denote by $Su_c = b$ the linear system (3.8), whose variables are the values at the solution centers Ω_c . Recall that each row of the matrix S is composed by zero elements except for the weights, (centers), corresponding to each disk D^k , that is, each row of size n_c , has only $n_c^{(k)}$ elements different from zero. Moreover, since $n_c \gg n_c^{(k)}$, the matrix S is sparse. To build the matrix S efficiently, i.e., to compute the weights, we can solve the following equations

$$A^{(k)}W_{\mathcal{J}}^{(k)}(x_1^{(k)}) = \mathcal{J}H^{(k)}(x_1^{(k)}), \quad k = 1, \dots, n_c. \quad (3.9)$$

Since the the matrix S is sparse standard solvers and preconditioners can be used. Besides, it is worth pointing out that by using the method of lines and a proper numerical time integrator, non stationary linear PDEs problems can be solve by the LHI method. To review exhaustively the LHI method, the interested reader can see [SPLM11, Fas07] and references therein.

4 Divergence free global method for evolutionary problems

In this section we present two methods for solving the time dependency for the unsteady Stokes system. The spatial dependency follows divergence-free RBF approximation like in [Wen09]. Let us define $L(\mathbf{y}, p) = -\mu\Delta\mathbf{y} + \nabla p$ and consider the system

$$\begin{cases} \mathbf{y}_t + L(\mathbf{y}, p) = \mathbf{f} & \text{in } Q, \\ \nabla \cdot \mathbf{y} = 0 & \text{in } Q, \\ B\mathbf{y} = \mathbf{g} & \text{on } \Sigma, \\ \mathbf{y}(\cdot, 0) = \mathbf{y}_0(\cdot) & \text{in } Q, \end{cases} \quad (4.1)$$

where B represents only one boundary operator describing (2.3).

4.1 Time backward scheme: global RBF collocation

The goal is to create a modified PDE-operator via a finite difference approximation for the time derivative, where the left-hand side is unknown and right-hand side is known. The time scheme follows some ideas by [SPLM11]. In order to illustrate this method we use backward finite differences (BFD) methods that are appropriate for the Stokes equations. The formulation at any time step for the system (4.1) is given as follows:

$$\begin{cases} \mathbf{y}^{n+s} + \Delta t \beta_s L(\mathbf{y}^{n+s}, p^{n+s}) = \Delta t \beta_s \mathbf{f}^{n+s} + \sum_{k=0}^{s-1} \sigma_k \mathbf{y}^{n+k} & \text{in } Q, \\ \nabla \cdot \mathbf{y}^{n+s} = 0 & \text{in } Q, \\ B\mathbf{y}^{n+s} = \mathbf{g}^{n+s} & \text{on } \Sigma, \end{cases} \quad (4.2)$$

where β_s, σ_k are known parameters within BFD methods. Thus, at each step we solve the following modified PDE

$$\begin{cases} \bar{L}(\mathbf{y}^{n+s}, p^{n+s}) = \mathbf{F}^{n+s} & \text{in } Q, \\ \nabla \cdot \mathbf{y}^{n+s} = 0 & \text{in } Q, \\ B\mathbf{y}^{n+s} = \mathbf{g}^{n+s} & \text{on } \Sigma, \end{cases} \quad (4.3)$$

where the source term is computed using previous steps and $\bar{L}, \mathbf{F}^{n+s}$ are defined by

$$\bar{L}(\mathbf{y}^{n+s}, p^{n+s}) := \mathbf{y}^{n+s} + \Delta t \beta_s L(\mathbf{y}^{n+s}, p^{n+s}), \quad \mathbf{F}^{n+s} := \Delta t \beta_s \mathbf{f}^{n+s} + \sum_{k=0}^{s-1} \sigma_k \mathbf{y}^{n+k}.$$

The field \mathbf{y}^{n+s} is then approximate by a linear combination of the divergence-free matrix-valued kernel $\Phi_{Div} = \nabla \times \Delta \times \psi = \{-\Delta I + \nabla \nabla^T\} \psi$, where Δ is the Laplacian, I is the identity matrix and $\psi : \mathbb{R}^d \rightarrow \mathbb{R}$ is a positive definitive function. Following [Wen09], the velocity pressure vector $(\mathbf{y}^{n+1}, p^{n+1})$ can be approximate by a linear combination of:

$$\Phi = \begin{bmatrix} \Phi_{Div} & 0 \\ 0 & \phi \end{bmatrix} : \mathbb{R}^d \rightarrow \mathbb{R}^{(d+1) \times (d+1)},$$

where $\phi : \mathbb{R}^d \rightarrow \mathbb{R}$ is a positive definitive function.

On the other hand, using the generalized interpolation collocation method, see [Wen04], The RBF ansatz, using Navier-slip boundary conditions (see (2.3)–(b)), is given by

$$(\hat{\mathbf{y}}^{n+s}, \hat{p}^{n+s})(\mathbf{x}) = \sum_{i=1}^d \sum_{j=1}^{n_b} (B_{ij}) \Phi(\mathbf{x} - \mathbf{z}) \alpha_{ij}^B + \sum_{i=1}^d \sum_{j=1}^{n_{in}} (\overline{L_{ij}}) \Phi(\mathbf{x} - \mathbf{z}) \alpha_{ij}^L, \quad (4.4)$$

where n_b, n_{in} are the total numbers of boundary and interior nodes respectively, $\alpha = (\alpha_{ij}^B, \alpha_{ij}^L) \in \mathbb{R}^{d(n_b+n_{in})}$ and $B_{ij}, \overline{L_{ij}}$ are vector-valued functionals defined as follows:

$$\overline{L_{ij}} = \delta_{\mathbf{x}_j^{in}} e_i + \beta_s \Delta t (\delta_{\mathbf{x}_j^{in}} \circ -\mu \Delta e_i + \delta_{\mathbf{x}_j^{in}} \circ \partial_i e_{d+1}) \quad (4.5)$$

and B_{ij} is

$$\delta_{\mathbf{x}_j^b} \sum_{k=1}^d e_k \nu_k \text{ for } i = 1 \quad \text{and} \quad \delta_{\mathbf{x}_j^b} \circ \mu \sigma(\bar{e}_d, e_{d+1}) \boldsymbol{\nu} \cdot \boldsymbol{\tau}_{i-1}, \text{ for } i = 2 \dots d \quad (4.6)$$

where $\boldsymbol{\nu}$ the outward unit normal vector to Ω , $\bar{e}_d = (e_1, \dots, e_d)$ and $(\tau_1, \dots, \tau_{d-1})$ is orthonormal basis of the tangent space.

Now, in order to simplify the notation, we shall proceed our analysis in 2D by defining the vector value function $(\phi^{B_1}, \phi^{B_2}, \phi^{\overline{L_1}}, \phi^{\overline{L_2}})$ such that the ansatz (4.4) can be rewritten in the form

$$\begin{aligned} (\hat{\mathbf{y}}^{n+s}, \hat{\mathbf{p}}^{n+s})(\mathbf{x}) &= \sum_{j=1}^{n_b} \phi^{B_1}(\mathbf{x} - \mathbf{x}_j^b) \alpha_{1j}^B + \sum_{j=1}^{n_b} \phi^{B_2}(\mathbf{x} - \mathbf{x}_j^b) \alpha_{2j}^B \\ &\quad + \sum_{j=1}^{n_{in}} \phi^{\overline{L_1}}(\mathbf{x} - \mathbf{x}_j^{in}) \alpha_{1j}^L + \sum_{j=1}^{n_{in}} \phi^{\overline{L_2}}(\mathbf{x} - \mathbf{x}_j^{in}) \alpha_{2j}^L. \end{aligned} \quad (4.7)$$

Once that the ansatz has been replaced in (4.3), we obtain the discrete system

$$H_+ \bar{\alpha}^{n+s} = \begin{pmatrix} \mathbf{F}^{n+s} \\ \mathbf{g}^{n+s} \end{pmatrix}, \quad (4.8)$$

where the collocation matrix H_+ is given by:

$$H_+ = \begin{pmatrix} \overline{L_1} \phi^{B_1} & \overline{L_1} \phi^{B_2} & \overline{L_1} \phi^{\overline{L_1}} & \overline{L_1} \phi^{\overline{L_2}} \\ \overline{L_2} \phi^{B_1} & \overline{L_2} \phi^{B_2} & \overline{L_2} \phi^{\overline{L_1}} & \overline{L_2} \phi^{\overline{L_2}} \\ B_1 \phi^{B_1} & B_1 \phi^{B_2} & B_1 \phi^{\overline{L_1}} & B_1 \phi^{\overline{L_2}} \\ B_2 \phi^{B_1} & B_2 \phi^{B_2} & B_2 \phi^{\overline{L_1}} & B_2 \phi^{\overline{L_2}} \end{pmatrix}.$$

Remark 4.1. In the case of Dirichlet boundary conditions, the vector-value functional B_{ij} defined in (4.6) is replaced by $B_{ij} = \delta_{\mathbf{x}_j} e_i$, and the collocation matrix H_+ is similar to the previous one.

4.2 Stability analysis

In this subsection, we proceed to present the stability analysis associated to the previous scheme, by using a matrix method similar to the procedure developed in [CDN06]. First, using equation (4.7) we define the interpolation matrix $A \in \mathbb{R}^{(n_{in}+n_b) \times (n_{in}+n_b)}$ such that

$$A \bar{\alpha}^{n+s} = \begin{pmatrix} M_{\phi_{in}} \\ M_{\phi_b} \end{pmatrix} \bar{\alpha}^{n+s} = (y^{n+s}(x_1^{in}), \dots, y^{n+s}(x_{n_{in}}^{in}), y^{n+s}(x_1^b), \dots, y^{n+s}(x_{n_b}^b))^T, \quad (4.9)$$

where $M_{\phi_{in}} \in \mathbb{R}^{n_{in} \times (n_{in}+n_b)}$, $M_{\phi_b} \in \mathbb{R}^{n_b \times (n_{in}+n_b)}$.

Following [CDN06], we define $H_- := \begin{pmatrix} M_{\phi_{in}} \\ 0 \end{pmatrix}$ and putting together (4.9) and (4.8) obtain

$$H_+ \bar{\alpha}^{n+s} = H_- \sum_{k=0}^{s-1} \sigma_k \bar{\alpha}^{n+k} + \begin{pmatrix} \Delta t \mathbf{f}^{n+s} \\ \mathbf{g}^{n+s} \end{pmatrix}.$$

Thus, it follows that

$$\mathbf{y}^{n+s} = A H_+^{-1} H_- A^{-1} \sum_{k=0}^{s-1} \sigma_k \mathbf{y}^{n+k} + A H_+^{-1} \begin{pmatrix} \Delta t \mathbf{f}^{n+s} \\ \mathbf{g}^{n+s} \end{pmatrix}.$$

Denoting by \mathbf{y}^n the exact solution and by $\hat{\mathbf{y}}^n$ the numerically computed solution, the error $\mathbf{e}^n = \mathbf{y}^n - \hat{\mathbf{y}}^n$ satisfies the equation

$$\mathbf{e}^{n+s} = K \sum_{k=0}^{s-1} \sigma_k \mathbf{e}^{n+k} + E_{n+s},$$

where E_{n+s} is the local error in the scheme (4.8) and $K = AH_+^{-1}H_-A^{-1}$. Besides, since E_{n+s} is small and therefore bounded, the error analysis can be analyzed using the equation

$$\mathbf{e}^{n+s} = K \sum_{k=0}^{s-1} \sigma_k \mathbf{e}^{n+k}.$$

By assuming that K is diagonalizable, i.e., $K = D^{-1}\Lambda D$, we can define $\mathbf{z}^n := D\mathbf{e}^n$ and therefore (4.2) is equivalent to

$$\mathbf{z}^{n+s} = \Lambda \sum_{k=0}^{s-1} \sigma_k \mathbf{z}^{n+k}.$$

Since Λ is a diagonal matrix, for every $j = 1, \dots, d(n_b + n_{in})$ we have that $z_j^{n+s} = \sum_{k=0}^{s-1} \lambda_j \sigma_k z_j^{n+k}$,

and whose solution is given by $z_j^n = \sum_{k=0}^{s-1} C_k^j r_k^n$, where C_k^j are arbitrary complex constants and r_k are the roots of the associated polynomial of the finite difference equation.

Finally, since $\|\mathbf{e}^n\|$ goes to zero iff $\|\mathbf{z}^n\|$ tends to zero, the method will be stable as long as the eigenvalues of K belong to the stability region of

$$\pi(r, \lambda) = r^s - \sum_{k=0}^{s-1} \lambda \sigma_k r^k. \quad (4.10)$$

As a consequence of the boundary locus technique [Lam91], we can deduce the following stability regions:

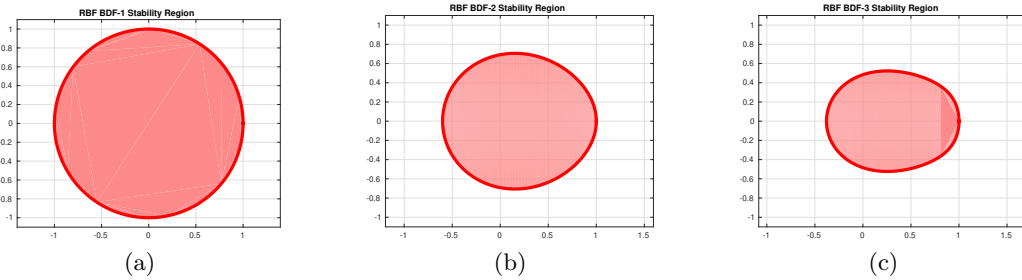


Figure 4.1: Stability regions using backward finite differences (BDF): a) nivel one, b) two levels and c) three levels.

4.3 The method of lines: global collocation

From the ansatz for the steady Stokes system, (4.4), we develop a numerical approach for the unsteady Stokes system with either Navier-slip or Dirichlet boundary conditions based in the method of lines to separate the variables in our approximation. Then, following the scheme carried out in the previous section, our ansatz is defined by:

$$(\hat{\mathbf{y}}, \hat{p})(\mathbf{x}, t) = \sum_{i=1}^d \sum_{j=1}^{n_b} (B_{ij}) \Phi(\mathbf{x} - \mathbf{z}) \alpha_{ij}^B(t) + \sum_{i=1}^d \sum_{j=1}^{n_{in}} (L_{ij}) \Phi(\mathbf{x} - \mathbf{z}) \alpha_{ij}^L(t),$$

with certain coefficients $\bar{\alpha}(t) = (\alpha_{ij}^B(t), \alpha_{ij}^L(t)) \in \mathbb{R}^{d(n_b + n_{in})}$, L_{ij} is given by

$$L_{ij} = \delta_{\mathbf{x}_j} \circ -\mu \Delta e_i + \delta_{\mathbf{x}_j} \circ \partial_i e_{d+1},$$

meanwhile B_{ij} is defined as in (4.6). In a similar way to Section 4.1, we develop this method in 2D and consider the vector value function $(\phi^{B_1}, \phi^{B_2}, \phi^{L_1}, \phi^{L_2})$ satisfying

$$\begin{aligned} (\hat{\mathbf{y}}, \hat{p})(\mathbf{x}, t) = & \sum_{j=1}^{n_b} \phi^{B_1}(\mathbf{x} - \mathbf{x}_j^b) \alpha_{1j}^B(t) + \sum_{j=1}^{n_b} \phi^{B_2}(\mathbf{x} - \mathbf{x}_j^b) \alpha_{2j}^B(t) \\ & + \sum_{j=1}^{n_{in}} \phi^{L_1}(\mathbf{x} - \mathbf{x}_j^{in}) \alpha_{1j}^L(t) + \sum_{j=1}^{n_{in}} \phi^{L_2}(\mathbf{x} - \mathbf{x}_j^{in}) \alpha_{2j}^L(t). \end{aligned}$$

Putting the ansatz above in the Stokes system, we obtain the following scheme

$$\begin{cases} \hat{\mathbf{y}}_t + L(\hat{\mathbf{y}}, \hat{p}) = \mathbf{f} & \text{in } Q, \\ \mathbf{B}\hat{\mathbf{y}} = \mathbf{g} & \text{on } \Sigma, \\ \hat{\mathbf{y}}(\cdot, 0) = \mathbf{y}_0(\cdot) & \text{in } Q, \end{cases} \quad (4.11)$$

which implies the system of ODEs

$$\begin{aligned} M_\phi \frac{d\bar{\alpha}(t)}{dt} + M_{L_\phi} \bar{\alpha}(t) &= \mathbf{f}, \\ M_{B_\phi} \bar{\alpha}(t) &= \mathbf{g}, \end{aligned}$$

where, for $\phi = [\phi_1, \phi_2]$, we have that $M_\phi, M_{L_\phi} \in \mathcal{M}((2n_{in}) \times (2n_b + 2n_{in}); \mathbb{R})$ and are defined as follows:

$$M_\phi = \begin{pmatrix} \phi_1^{B_1} & \phi_1^{B_2} & \phi_1^{L_1} & \phi_1^{L_2} \\ \phi_2^{B_1} & \phi_2^{B_2} & \phi_2^{L_1} & \phi_2^{L_2} \end{pmatrix}, \quad M_{L_\phi} = \begin{pmatrix} L_1 \phi^{B_1} & L_1 \phi^{B_2} & L_1 \phi^{L_1} & L_1 \phi^{L_2} \\ L_2 \phi^{B_1} & L_2 \phi^{B_2} & L_2 \phi^{L_1} & L_2 \phi^{L_2} \end{pmatrix}$$

and $M_{B_\phi} \in \mathcal{M}(2n_b \times (2n_b + 2n_{in}); \mathbb{R})$

$$M_{B_\phi} = \begin{pmatrix} B_1 \phi^{B_1} & B_1 \phi^{B_2} & B_1 \phi^{L_1} & B_1 \phi^{L_2} \\ B_2 \phi^{B_1} & B_2 \phi^{B_2} & B_2 \phi^{L_1} & B_2 \phi^{L_2} \end{pmatrix}.$$

Finally, we use BDF methods for solving the former system of ODEs, thus, at each step we solve the following linear system:

$$\begin{pmatrix} M_\phi + \Delta t \beta_s M_{L_\phi} \\ M_{B_\phi} \end{pmatrix} \bar{\alpha}^{n+s} = \begin{pmatrix} \Delta t \beta_s \mathbf{f}^{n+s} + \sum_{k=0}^{s-1} \sigma_k M_\phi \bar{\alpha}^{n+k} \\ \mathbf{g}^{n+s} \end{pmatrix}. \quad (4.12)$$

Since $M_\phi \bar{\alpha}(t_n) = \mathbf{y}^n$, the equation (4.12) is equivalent to

$$\begin{pmatrix} M_\phi + \Delta t \beta_s M_{L_\phi} \\ M_{B_\phi} \end{pmatrix} \bar{\alpha}^{n+s} = \begin{pmatrix} \Delta t \beta_s \mathbf{f}^{n+s} + \sum_{k=0}^{s-1} \sigma_k \mathbf{y}^{n+k} \\ \mathbf{g}^{n+s} \end{pmatrix}. \quad (4.13)$$

Remark 4.2. As in subsection 4.2, we proceed to present an analysis of the stability for the method introduced in this subsection. From system (4.13), we can deduce

$$\mathbf{y}^{n+s} = A H_+^{-1} H_- A^{-1} \sum_{k=0}^{s-1} \sigma_k \mathbf{y}^{n+k} + A H_+^{-1} \begin{pmatrix} \Delta t \mathbf{f}^{n+s} \\ \mathbf{g}^{n+s} \end{pmatrix}.$$

Where A is defined as in equation (4.9) and :

$$H_+ = \begin{pmatrix} M_\phi + \Delta t \beta_s M_{L_\phi} \\ M_{B_\phi} \end{pmatrix} \quad H_- = \begin{pmatrix} M_\phi \\ 0 \end{pmatrix}$$

Therefore, the method will be stable as long as the eigenvalues of $K = A H_+^{-1} H_- A^{-1}$ are in the stability region of (4.10).

4.4 Numerical examples: line method BDF2

In the sequel, we evaluate the accuracy of the previous scheme through BDF2. The objective is test the feasibility of the schemes by considering either nonhomogeneous Dirichlet conditions or nonhomogeneous Navier–slip conditions on the system (4.1). In order to generate the divergence free kernel we use inverse multi quadric (MQ), with a shape parameter $c = 0.1$. Since this type of kernel are very ill conditioned we have used the Matlab package ADVANPIX for multi precision calculus and set the number of digits to 50. In this subsection, all the computations are done in the programming languages Matlab and FreeFemm++. We introduce a uniform mesh generate by means of the package DISTMESH, where the total number of nodes is 362.

Let Ω be the unit circle, i.e., $\Omega = \{(x, y) \in \mathbb{R}^2 : x^2 + y^2 < 1\}$, the analytical solution of (4.1) given by

$$(\mathbf{y}_1(x, y, t), \mathbf{y}_2(x, y, t)) = \left(-\pi y \sin\left(\frac{\pi}{2}(x^2 + y^2)\right) \sin(\pi t), \pi x \sin\left(\frac{\pi}{2}(x^2 + y^2)\right) \sin(\pi t) \right)$$

and pressure $p(x, y, t) = \sin(x - y + t)$. We compare the error in velocity and pressure in the L^∞ -norm between the exact and numerical solutions for several time steps Δt . The errors are denoted by $\epsilon_{\mathbf{y}} = \mathbf{y}_{exact} - \mathbf{y}_{approx}$ and $\nabla \epsilon_{\mathbf{p}} = \nabla p_{exact} - \nabla p_{approx}$, respectively. The results are presented in Table 4.1 and Figure 4.2.

B.C	Dirichlet		Navier-slip	
Δt	$\ \epsilon_{\mathbf{y}}\ _\infty$	$\ \nabla \epsilon_{\mathbf{p}}\ _\infty$	$\ \epsilon_{\mathbf{y}}\ _\infty$	$\ \nabla \epsilon_{\mathbf{p}}\ _\infty$
$\mu = 1$				
0.1	8.570E-03	1.28E-06	9.23E-02	1.42E-04
0.01	9.32E-05	4.53E-07	8.00E-04	1.43E-04
0.002	3.74E-06	9.76E-07	4.39E-05	1.43E-04
0.001	9.37E-07	6.33E-07	2.36E-05	1.43E-04
0.0002	3.74E-08	4.53E-07	1.97E-05	1.43E-04
0.0001	9.32E-09	4.53E-07	1.96E-05	1.43E-04
5e-05	5.24E-09	4.53E-07	1.96E-05	1.43E-04
$\mu = 10^{-6}$				
0.1	1.10E-01	1.06E-02	1.10E-01	3.61E-04
0.01	9.48E-04	1.09E-04	9.79E-04	3.57E-04
0.002	3.72E-05	6.38E-06	1.48E-04	3.81E-04
0.001	9.29E-06	1.94E-06	1.41E-04	3.86E-04
0.0002	3.70E-07	9.45E-08	1.39E-04	3.86E-04
0.0001	9.31E-08	1.91E-08	1.39E-04	3.85E-04
5e-05	2.46E-08	1.84E-08	1.39E-04	3.85E-04
$\mu = 10^{-3}$				

Table 4.1: Convergence behaviour of velocity and pressure in the L^∞ -norm using inverse MQ, 362 nodes and different viscosity coefficients μ .

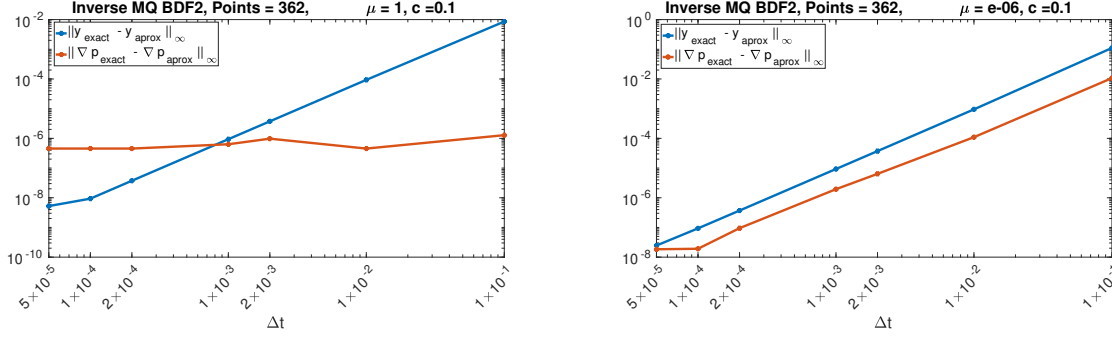


Figure 4.2: Convergence behaviour of $\|\epsilon(\mathbf{y})\|_\infty$ (blue) and $\|\nabla\epsilon(\mathbf{p})\|_\infty$ (red) in the 2D test, Dirichlet boundary conditions. The left-hand side with $\mu = 1$, meanwhile in the right-hand side $\mu = 1 \times 10^{-6}$.

In the left-hand side of figure 4.2 can be observed that the pressure remains almost constant, this result was obtained by Fuselier in their experiments, [FSW16]. A possible explanation to this behavior is that the convergence of the pressure, which we think it should depend on the fill distance, the shape parameter and the viscosity is lower bounded. In fact, in the right-hand side of figure 4.2 where the viscosity μ is of the order of 10^{-6} , the pressure decay with almost the same slope as the velocity and it becomes constant after the time step less than 10^{-4} .

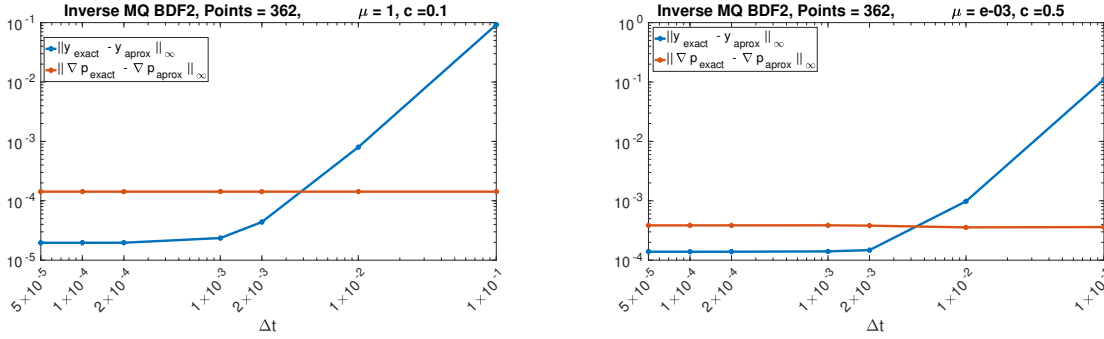


Figure 4.3: Convergence behaviour of $\|\epsilon(\mathbf{y})\|_\infty$ (blue) and $\|\nabla\epsilon(\mathbf{p})\|_\infty$ (red) by considering Navier-slip boundary conditions and two different values of viscosity μ and shape parameter c .

Figure 4.3 shows the convergence behaviour of $\|\epsilon(\mathbf{y})\|_\infty$ and $\|\nabla\epsilon(\mathbf{p})\|_\infty$ by putting Navier-slip boundary conditions. Observe that different bounds are obtained in this case, depending again on the fill distance, the shape parameter and the viscosity. Indeed, if we change the shape parameter for the right figure by $c = 0.1$, the convergence is not reached. It may be a hidden condition of the style of CFL condition. Numerically, this can be explained by noting that some eigenvalues lies outside the stability region, see figure 4.4.

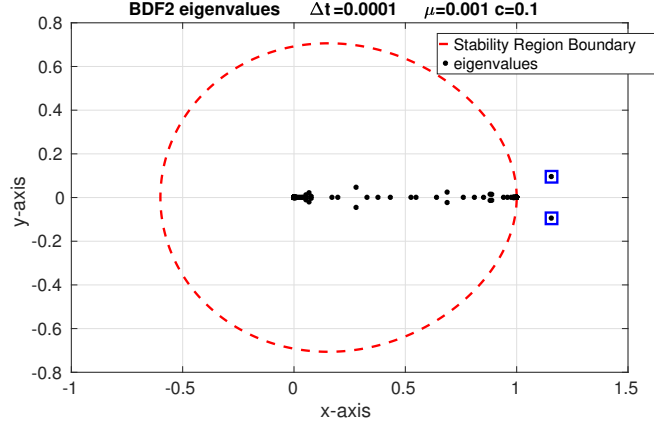


Figure 4.4: Eigenvalues of the matrix $K = AH_+^{-1}H_-A^{-1}$ defined in subsection 4.2 concerning stability analysis. The blue squares represent the eigenvalues located outside the stability region. Here, Navier-Slip boundary conditions were imposed.

5 LHI method for the Stokes system

In this section we formulate a RBF–LHI vectorial technique for the unsteady Stokes system based on the scalar LHI algorithm, see introduction. First, the numerical description for the steady Stokes system is formulated and a numerical example is presented. Once completed the steady case, we apply the time advancement scheme given in subsection 4.1 for obtaining an implicit discretization scheme. A stability analysis is also carried out.

5.1 Steady problem

From [Wen09], the vectorial LHI-algorithm for the system

$$\begin{cases} -\mu\Delta\mathbf{y} + \nabla p = \mathbf{F} & \text{in } Q, \\ \nabla \cdot \mathbf{y} = 0 & \text{in } Q, \\ +BC & \text{on } \Sigma, \end{cases} \quad (5.1)$$

where \mathbf{F} is known and $+BC$ indicates the boundary conditions (see (2.3)), reads as follows: let us define a vector $\mathbf{u} := (\mathbf{u}_n, u_{n+1}) = (\mathbf{y}, p) \in \mathbb{R}^{d+1}$. and operators $\mathcal{L}, \mathcal{B}, \mathcal{B}_1, \mathcal{B}_2$ such that the right-hand side of (5.1) is given by

$$\mathcal{L}\mathbf{u} := -\mu\Delta\mathbf{u}_n + \nabla u_{n+1} = (-\mu\Delta, \nabla) \cdot (\mathbf{u}_n, u_{n+1}); \quad \nabla \cdot \mathbf{u}_n = 0$$

and either

$$\underbrace{\mathcal{B}\mathbf{u} := \mathbf{u}_n}_{\text{Dirichlet}} \quad \text{or} \quad \underbrace{\mathcal{B}_1\mathbf{u} := (\sigma(\mathbf{u}_n, u_{n+1})\boldsymbol{\nu})_{tg} = (\sigma(\mathbf{u})\boldsymbol{\nu})_{tg}; \quad \mathcal{B}_2\mathbf{u} = \mathbf{u}_n \cdot \boldsymbol{\nu}}_{\text{Navier-slip}} \quad (5.2)$$

As previously, for each disk D^k with center x_1^k , we must define a local sub-system (see introduction):

$$\begin{cases} \mathbf{u}(x_i) = \bar{h}_i & \text{in } \Omega_{sc}^k \subset \Omega_{sc} \cap D^k, \\ \mathcal{L}\mathbf{u} = \mathbf{F} & \text{in } \Omega_{pdec}^k \subset \Omega_{pdec} \cap D^k, \\ (5.2) & \text{on } \Omega_{fc}^k \subset \Omega_{fc} \cap D^k. \end{cases} \quad (5.3)$$

In order to solve the systems (5.3) we first define the matrix-valued kernel

$$\mathbf{\Phi} = \begin{bmatrix} \mathbf{\Phi}_{Div} & 0 \\ 0 & \psi \end{bmatrix} : \mathbb{R}^d \rightarrow \mathbb{R}^{(d+1) \times (d+1)},$$

where $\mathbf{\Phi}_{Div} = \Delta \times \nabla \times \psi = \{-\Delta I + \nabla \nabla^T\} \psi(\mathbf{x}) : \mathbb{R}^d \rightarrow \mathbb{R}^{d+1}$ is a divergence-free positive definite kernel, Δ is the Laplacian, I the identity matrix, and ϕ, ψ are global C^∞ positive definite scalar RBFs.

Since we are choosing free divergence radial kernel, the incompressibility equation is missing, and therefore we lack a differential operator. In order to obtain a fully sparse system from (3.9), we include the pressure as unknown variable in the local system (5.3). This leads to the following local system

$$\begin{cases} \mathbf{u}_n(x_i) = \bar{h}_i & \text{in } \Omega_{sc}^k, \\ \mathcal{L}\mathbf{u} = \mathbf{F} & \text{in } \Omega_{pdec}^k, \\ (5.2) & \text{on } \Omega_{fc}^k. \end{cases} \quad (5.4)$$

Using the generalized interpolation collocation method [Wen04], the ansatz by considering Navier-slip boundary conditions (see (5.2)) is given by

$$\begin{aligned} (\hat{y}^{(k)}, \hat{p}^{(k)})(\mathbf{x}) &= \sum_{i=1}^d \sum_{j=1}^{n_{sc}^k} (I_{ij}^k) \mathbf{\Phi}(\mathbf{x} - \mathbf{z}) \alpha_{ij}^{I^k} + \sum_{i=1}^{d+1} \sum_{j=1}^{n_{fc}^k} (B_{ij}^k) \mathbf{\Phi}(\mathbf{x} - \mathbf{z}) \alpha_{ij}^{B^k} \\ &\quad + \sum_{i=1}^d \sum_{j=1}^{n_{pdec}^k} (L_{ij}^k) \mathbf{\Phi}(\mathbf{x} - \mathbf{z}) \alpha_{ij}^{L^k}, \end{aligned}$$

where $\bar{\alpha} = (\alpha_{ij}^{I^k}, \alpha_{ij}^{B^k}, \alpha_{ij}^{L^k}) \in \mathbb{R}^{d(n_{sc}^k + n_{fc}^k + n_{pdec}^k)}$, $I_{ij}^k := \delta_{\mathbf{x}_j^{sc(k)}} e_i$, B_{ij}^k are vector-valued functionals defined like in (4.6), and $L_{ij}^k := \delta_{\mathbf{x}_j^{sc(k)}} \circ -\mu \Delta e_i + \delta_{\mathbf{x}_j^{sc(k)}} \circ \partial_i e_{d+1}$.

Now, in order to simplify the notation, we shall proceed our analysis by defining the vector value function $(\phi^{I_1}, \phi^{I_2}, \phi^{B_1}, \phi^{B_2}, \phi^{L_1}, \phi^{L_2})$, such that the ansatz above can be rewritten in the form

$$\begin{aligned} (\hat{y}^{(k)}, \hat{p}^{(k)})(\mathbf{x}) &= \sum_{j=1}^{n_{sc}^k} \phi^{I_1}(\mathbf{x} - \mathbf{x}_j^{sc(k)}) \alpha_{1j}^{I_1} + \sum_{j=1}^{n_{sc}^k} \phi^{I_2}(\mathbf{x} - \mathbf{x}_j^{sc(k)}) \alpha_{2j}^{I_2} \\ &\quad + \sum_{j=1}^{n_{fc}^k} \phi^{B_1}(\mathbf{x} - \mathbf{x}_j^{fc(k)}) \alpha_{1j}^{B_1} + \sum_{j=1}^{n_{fc}^k} \phi^{B_2}(\mathbf{x} - \mathbf{x}_j^{fc(k)}) \alpha_{2j}^{B_2} \\ &\quad + \sum_{j=1}^{n_{pdec}^k} \phi^{L_1}(\mathbf{x} - \mathbf{x}_j^{pdec(k)}) \alpha_{1j}^{L_1} + \sum_{j=1}^{n_{pdec}^k} \phi^{L_2}(\mathbf{x} - \mathbf{x}_j^{pdec(k)}) \alpha_{2j}^{L_2}. \end{aligned} \quad (5.5)$$

Putting ansatz (5.5) in the local Stokes system (5.4), we obtain the local Gram matrix

$$A^{(k)} = \begin{pmatrix} I_1 \phi^{I_1} & I_1 \phi^{I_2} & I_1 \phi^{B_1} & I_1 \phi^{B_2} & I_1 \phi^{L_1} & I_1 \phi^{L_2} \\ I_2 \phi^{I_1} & I_2 \phi^{I_2} & I_2 \phi^{B_1} & I_2 \phi^{B_2} & I_2 \phi^{L_1} & I_2 \phi^{L_2} \\ B_1 \phi^{I_1} & B_1 \phi^{I_2} & B_1 \phi^{B_1} & B_1 \phi^{B_2} & B_1 \phi^{L_1} & B_1 \phi^{L_2} \\ B_2 \phi^{I_1} & B_2 \phi^{I_2} & B_2 \phi^{B_1} & B_2 \phi^{B_2} & B_2 \phi^{L_1} & B_2 \phi^{L_2} \\ L_1 \phi^{I_1} & L_1 \phi^{I_2} & L_1 \phi^{B_1} & L_1 \phi^{B_2} & L_1 \phi^{L_1} & L_1 \phi^{L_2} \\ L_2 \phi^{I_1} & L_2 \phi^{I_2} & L_2 \phi^{B_1} & L_2 \phi^{B_2} & L_2 \phi^{L_1} & L_2 \phi^{L_2} \end{pmatrix}, \quad (5.6)$$

which in turn let us to compute the weights by solving the following system

$$\begin{cases} A^{(k)} W_{L_1}^{(k)} \begin{pmatrix} x_1^{sc(k)} \end{pmatrix} = L_1 H^{(k)}(x_1^{sc(k)}), & k = 1, \dots, n_{sc}, \\ A^{(k)} W_{L_2}^{(k)} \begin{pmatrix} x_1^{sc(k)} \end{pmatrix} = L_2 H^{(k)}(x_1^{sc(k)}), & k = 1, \dots, n_{sc}, \end{cases}$$

where $H^{(k)}(x)$ in this case is given by:

$$H^{(k)}(x) = \begin{pmatrix} \phi^{I_1}(\|x - x^{sc(k)}\|) \\ \phi^{I_2}(\|x - x^{sc(k)}\|) \\ \phi^{B_1}(\|x - x^{fc(k)}\|) \\ \phi^{B_2}(\|x - x^{fc(k)}\|) \\ \phi^{L_1}(\|x - x^{pdec(k)}\|) \\ \phi^{L_2}(\|x - x^{pdec(k)}\|) \end{pmatrix}.$$

Once the weights are known, we can build the sparse global matrix from the following system

$$\begin{cases} W_{L_1}^{(k)} \begin{pmatrix} x_1^{sc(k)} \end{pmatrix} d^{(k)} = F_1(x_1^{sc(k)}) & k = 1, \dots, n_{sc}, \\ W_{L_2}^{(k)} \begin{pmatrix} x_1^{sc(k)} \end{pmatrix} d^{(k)} = F_2(x_1^{sc(k)}) & k = 1, \dots, n_{sc}, \end{cases}$$

where

$$d^{(k)} = \left(y_1(x^{sc(k)}), y_2(x^{sc(k)}), g_1(x^{fc(k)}), g_2(x^{fc(k)}), F_1(x^{pdec(k)}), F_2(x^{pdec(k)}) \right)^T.$$

It is important to highlight that in order to avoid singularity of the sparse system we need that $x_1^{sc(k)} \notin \Omega_{pdec}^k$, see framework by [SPLM11].

Remark 5.1. Analogous to Remark 4.1, by considering Dirichlet boundary conditions, the vector $\bar{\alpha}$ belongs to $\mathbb{R}^{d(n_{sc}^k + n_{pdec}^k)}$, since B_{ij} is replaced by $B_{ij} = \delta_{x_j} e_i$, and in consequence the local Gram matrix $A^{(k)}$ is akin to the previous one. In the next numerical example we test such boundary conditions and postpone numerical experiments concerning the Navier-slip conditions until subsection 5.4.

5.2 Numerical result: stationary case

Here, the numerical example on an unitary square described in [Wen09] is used to examine the convergence of our method with nonhomogeneous Dirichlet boundary conditions. We have used advanpix package to super pass the ill condition Gram matrix. Thus, for $\Omega = (0,1) \times (0,1)$ and $\mu = 1$, we consider the following analytical solution to (5.1): $\mathbf{u}(\mathbf{x}) = (20x_1x_2^3, 5x_1^4 - 5x_2^4)$, $p(\mathbf{x}) = 60x_1^2x_2 - 20x_2^3$. Non-dimensional shape parameters c^* of values 1.0 and 0.01 are used throughout, as well as 25, 50, 80 local nodes for inverse MQ and Gaussian RBFs. Table 5.1 contains the approximation orders of the L^2 and L^∞ error of the velocity field, i.e., $\|\epsilon_{\mathbf{u}}\|_\infty := \|\mathbf{u}_{exact} - \mathbf{u}_{approx}\|_\infty$ and $\|\epsilon_{\mathbf{u}}\|_2 := \|\mathbf{u}_{exact} - \mathbf{u}_{approx}\|_2$.

Total nodes	Local nodes	c^*	$cond(A^k)$	$\ \epsilon_u\ _\infty$	$\ \epsilon_u\ _2$
400	50	1.0	3.77e+37	4.78e-08	2.74e-07
1225	25	1.0	2.94e+32	5.49e-06	1.10e-04
1225	80	1.0	2.99e+52	9.34e-15	8.31e-14
400	50	1.0	1.13e+26	0.000485214	0.00291627
1225	25	1.0	5.15e+25	1.09e-02	1.94e-01
1225	25	0.01	2.46e+40	9.14e-09	1.63e-07
1225	80	1.0	4.65e+38	1.24e-07	1.41e-06

Table 5.1: Approximation errors of the velocity field for the steady Stokes problem using LHI method. Two shape parameters c^* are considered; top: Gaussian RBF; bottom: inverse MQ RBF.

5.3 Evolutionary problem

In this subsection we formulate a RBF–LHI vectorial technique for the evolutionary Stokes problem based in Section 4.1, which create a modified PDE operator using the finite difference method (FDM) for the time discretization, as well as BFD methods. Specifically, for the system

$$\begin{cases} \mathbf{y}_t + L(\mathbf{y}, p) = \mathbf{f} & \text{in } Q, \\ \nabla \cdot \mathbf{y} = 0 & \text{in } Q, \\ B\mathbf{y} = \mathbf{g} & \text{on } \Sigma, \\ \mathbf{y}(\cdot, 0) = \mathbf{y}_0(\cdot) & \text{in } Q, \end{cases} \quad (5.7)$$

where $L(\mathbf{y}, p) = -\mu\Delta\mathbf{y} + \nabla p$, we define the operator of left–hand side \bar{L} by

$$\bar{L}(\mathbf{y}^{n+s}, p^{n+s}) := \mathbf{y}^{n+s} + \Delta t \beta_s L(\mathbf{y}^{n+s}, p^{n+s})$$

and the source term

$$\mathbf{F}^{n+s} := \Delta t \beta_s \mathbf{f}^{n+s} + \sum_{k=0}^{s-1} \sigma_k \mathbf{y}^{n+k}.$$

Following the same procedure as in the stationary case, our ansatz is given by

$$\begin{aligned} (\hat{y}^{(n+2,k)}(\mathbf{x}), \hat{p}^{(n+2,k)}(\mathbf{x})) &= \sum_{j=1}^{n_{sc}^k} \phi^{I_1}(\mathbf{x} - \mathbf{x}_j^{sc(k)}) \alpha_{1j}^I + \sum_{j=1}^{n_{sc}^k} \phi^{I_2}(\mathbf{x} - \mathbf{x}_j^{sc(k)}) \alpha_{2j}^I \\ &+ \sum_{j=1}^{n_{fc}^k} \phi^{B_1}(\mathbf{x} - \mathbf{x}_j^{fc(k)}) \alpha_{1j}^B + \sum_{j=1}^{n_{fc}^k} \phi^{B_2}(\mathbf{x} - \mathbf{x}_j^{fc(k)}) \alpha_{2j}^B \\ &+ \sum_{j=1}^{n_{pdec}^k} \phi^{\bar{L}_1}(\mathbf{x} - \mathbf{x}_j^{pdec(k)}) \alpha_{1j}^L + \sum_{j=1}^{n_{pdec}^k} \phi^{\bar{L}_2}(\mathbf{x} - \mathbf{x}_j^{pdec(k)}) \alpha_{2j}^L, \end{aligned} \quad (5.8)$$

which is collocated in the local Stokes system

$$\begin{cases} \mathbf{u}_n(x_i) = \bar{h}_i & \text{in } \Omega_{sc}^k \subset \Omega_{sc} \cap D^k, \\ \bar{L}\mathbf{u} = \mathbf{F} & \text{in } \Omega_{pdec}^k \subset \Omega_{pdec} \cap D^k, \\ B\mathbf{u} = g & \text{on } \Omega_{fc}^k \subset \Omega_{fc} \cap D^k. \end{cases} \quad (5.9)$$

After that, we can obtain the local Gram matrix, which in turn let us to compute the weights. Once the weights are known, we can build a sparse global system using the system

$$\begin{cases} W_{L_1}^{(k)}(x_1^{sc(k)}) d^{(n+s,k)} = \Delta t \beta_s f_1^{n+s}(x_1^{sc(k)}) + \sum_{k=0}^{s-1} \sigma_k y_1^{n+k}(x_1^{sc(k)}), & k = 1, \dots, n_{sc}, \\ W_{L_2}^{(k)}(x_1^{sc(k)}) d^{(n+s,k)} = \Delta t \beta_s f_2^{n+s}(x_1^{sc(k)}) + \sum_{k=0}^{s-1} \sigma_k y_2^{n+k}(x_1^{sc(k)}), & k = 1, \dots, n_{sc}, \end{cases} \quad (5.10)$$

for each $x_1^{sc(k)}$ in D^k , and where $d^{(n+s,k)}$ is

$$(y_1^{(n+s)}(x^{sc(k)}), y_2^{(n+s)}(x^{sc(k)}), g_1^{n+s}(x^{fc(k)}), g_2^{n+s}(x^{fc(k)}), F_1^{n+s}(x^{pdec(k)}), F_2^{n+s}(x^{pdec(k)}))^T.$$

Observe that (5.10) can be expressed in matrix form as:

$$\begin{pmatrix} W_{L_1}^{y_1} & W_{L_1}^{y_2} & W_{L_1}^{B_1} & W_{L_1}^{B_2} & W_{L_1}^{L_1} & W_{L_1}^{L_2} \\ W_{L_2}^{y_1} & W_{L_2}^{y_2} & W_{L_2}^{B_1} & W_{L_2}^{B_2} & W_{L_2}^{L_1} & W_{L_2}^{L_2} \end{pmatrix} \begin{bmatrix} y_1^{n+s} \\ y_2^{n+s} \\ g_1^{n+s} \\ g_2^{n+s} \\ F_1^{n+s} \\ F_2^{n+s} \end{bmatrix} = \begin{bmatrix} F_1^{n+s} \\ F_2^{n+s} \end{bmatrix}, \quad (5.11)$$

where the functions F_1^{n+s}, F_2^{n+s} in the right-hand side of (5.11) are evaluated in every $x_1^{sc(k)}$ of D^k , meanwhile F_1^{n+s} and F_2^{n+s} in the left-hand side of (5.11) in $x^{pdec(k)}$. Thus, it allows to compute (y^{n+s}, p^{n+s}) .

Remark 5.2. *In a more general setting, we can establish an analysis of stability for the LHI method presented above. By simplicity, let us consider $x_1^{sc(k)} = x^{pdec(k)}$ on each disk D^k . Besides, let $\mathbf{e} := \mathbf{y} - \hat{\mathbf{y}}$ be the error between the exact and approximate solution in which we have discarded the local truncation error. Thus, (5.11) can be transformed for the error \mathbf{e}_n in the form*

$$\begin{pmatrix} W_{L_1}^{y_1} & W_{L_1}^{y_2} \\ W_{L_2}^{y_1} & W_{L_2}^{y_2} \end{pmatrix} \begin{bmatrix} e_1^{n+s} \\ e_2^{n+s} \end{bmatrix} = \begin{bmatrix} \sum_{k=0}^{s-1} \sigma_k e_1^{n+k} \\ \sum_{k=0}^{s-1} \sigma_k e_2^{n+k} \end{bmatrix} - \begin{pmatrix} W_{L_1}^{L_1} & W_{L_1}^{L_2} \\ W_{L_2}^{L_1} & W_{L_2}^{L_2} \end{pmatrix} \begin{bmatrix} \sum_{k=0}^{s-1} \sigma_k e_1^{n+k} \\ \sum_{k=0}^{s-1} \sigma_k e_2^{n+k} \end{bmatrix}.$$

Thus, $\mathbf{e}^{n+s} = S_1^{-1}(I - S_2)(\sum_{k=0}^{s-1} \sigma_k e^{n+k})$, where

$$S_1 = \begin{pmatrix} W_{L_1}^{y_1} & W_{L_1}^{y_2} \\ W_{L_2}^{y_1} & W_{L_2}^{y_2} \end{pmatrix} \quad \text{and} \quad S_2 = \begin{pmatrix} W_{L_1}^{L_1} & W_{L_1}^{L_2} \\ W_{L_2}^{L_1} & W_{L_2}^{L_2} \end{pmatrix}.$$

Therefore, the LHI method will be stable as long that eigenvalues of $S_1^{-1}(I - S_2)$ lie in the stability region of (4.10).

5.4 Numerical results: evolutionary case

From the theoretical description previously developed for the RBF-LHI method for the unsteady Stokes system, the present subsection shows numerical results of its implementation. We build the divergence free kernel by using inverse multi quadric (MQ) with a shape parameter $c = 0.1$ and again, the Matlab package ADVANPIX is considered. In this case, we introduce a uniform mesh generate by means of the package DISTMESH with 1312 total nodes. The viscosity

coefficient is $\mu = 1$. In order to test our numerical approach, we consider the following analytical solution to (5.7) over the unitary circle.

$$(\mathbf{y}_1(x, y, t), \mathbf{y}_2(x, y, t)) = \left(-\pi y \sin\left(\frac{\pi}{2}(x^2 + y^2)\right) \sin(\pi t), \pi x \sin\left(\frac{\pi}{2}(x^2 + y^2)\right) \sin(\pi t) \right)$$

and pressure $p(x, y, t) = \sin(x - y + t)$.

As in section 4.4, we compare the velocity error in the L^∞ -norm between the exact and numerical solutions, i.e., $\epsilon_y = \mathbf{y}_{exact} - \mathbf{y}_{approx}$. Here, we decide to omit the pressure error since an extra computation is needed to calculate. The results are presented in Table 5.2.

In addition to Table 5.2 where we note non-convergence cases, Figure 5.1 gives an answer about it. Figure 5.1 shows the eigenvalues of the matrix $S_1^{-1}(I - S_2)$ described in the previous section and its distribution over the stability region (SR). Indeed, we can appreciate that for the non-convergence cases the eigenvalues are located outside the SR of the BDF2 method ((4.10)), and therefore the stability condition is broken. That means again that there exists a hidden condition depending on the shape parameter, the diffusion coefficient, time-step, fill-distance and local-fill distance.

B.C	Dirichlet		Navier-slip	
Stencil Size	30	60	30	60
Δt	$\ \epsilon_y\ _\infty$		$\ \epsilon_y\ _\infty$	
0.02	3.72E-04	3.72E-04	3.07E-03	3.08E-03
0.01	9.36E-05	9.36E-05	7.85E-04	7.91E-04
0.005	2.35E-05	N.C	1.96E-04	2.01E-04
0.002	N.C	N.C	N.C	3.38E-05

Table 5.2: Convergence behaviour of velocity in the L^∞ -norm using inverse MQ. Non-convergence (N.C).

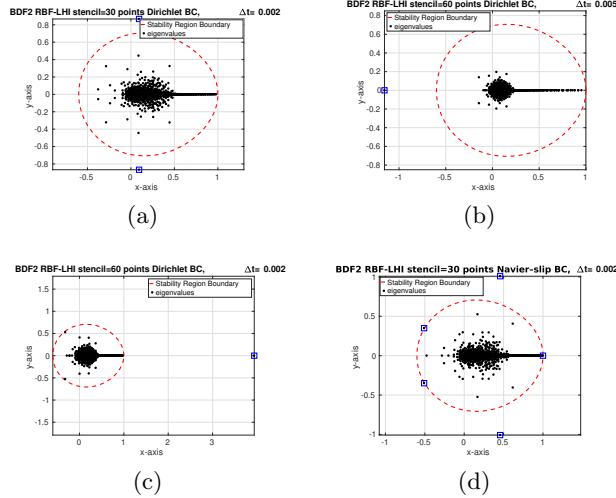


Figure 5.1: Representation of eigenvalues of the matrix $S_1^{-1}(I - S_2)$. The blue squares represent the eigenvalues located outside the stability region. The a) b) c) figures are associated to the Dirichlet boundary conditions and d) corresponds to the case of Navier-slip boundary conditions.

6 Numerical control problem

The approximate solution to the null controllability problem for the two-dimensional Stokes system with few scalar controls is carried out in this section. Hence, both Dirichlet and Navier-slip boundary conditions are considered. As mention before, the numerical implementation follows the method developed above through RBF-LHI, and simultaneously, those are compared against a mixed formulation using finite element method (FEM) for only the Dirichlet case, since the implementation of Navier-Slip is not straightforward with FEM. Although this is perfectly possible, the major problem is that both essential and natural boundary conditions should be incorporated within the algorithm to make it reliable. The shape of the domine, in our case a circle, makes this task more difficult.

Following [GLH08], the CGM is implemented with a stopping criteria of $\epsilon = 10^{-8}$ for solving the dual system (2.1), (2.7). We use the following data: $\Omega = \{(x, y) \in \mathbb{R}^2 : x^2 + y^2 < 1\}$, the observation set $\omega = \{(x, y) \in \mathbb{R}^2 : x^2 + y^2 < 0.25\}$, $T = 0.25$. The reason for this choice of T is that if we take $T = 1$, the solution with control force is very close to the solution without control, thus, it is difficult to appreciate the effect of the control in the numerical experiments.

In all cases, we use a uniform mesh of 3512 points generated with FreeFem++, the time step size is $\Delta t = \frac{1}{200}$ and diffusion coefficient $\mu = 1$. For the initial condition we choose $(y_1^0, y_2^0) = (-\pi y \cos(\frac{\pi}{2}(x^2 + y^2))^2, \pi x \cos(\frac{\pi}{2}(x^2 + y^2))^2)$. Regarding the functional (2.4), we set the regularization parameters $c_1 = 1/300$, $c_2^{-1} = 0$ by having controls with both non-zeros scalar component ($\mathbf{v} = (v_1, v_2)$) and $c_1^{-1} = 0$, $c_2 = 1/300$ by considering controls with one scalar control (either $\mathbf{v} = (v_1, 0)$ or $\mathbf{v} = (0, v_2)$).

Remark 6.1. *For the numerical experiments we use a triangular mesh for two specific reasons, the first one is to have a fair comparison between RBF-LHI and finite element, and the second is because CGM require to calculate integrals over the domain thus for LHI-RBF method it is more efficient to use the triangulation to calculate integrals with \mathcal{P}_1 -type elements.*

6.1 Divergence free RBF-LHI

To generate the divergence free kernel for the LHI method we use IMQ-RBF with a constant shape parameter $c = 0.1$. It's important to underline that the indicator function $\mathbb{1}_\omega$ given in the system (2.1) is approximate by the smooth function $1/(1 + \exp(-2k(0.5 - \|x\|_2)))$ with $k = 20$, otherwise our solution degenerate, which can be explained due to Gibbs phenomena.

Table 6.1 shows the number of iterations to achieve the stopping criteria $\epsilon = 10^{-8}$ in the CGM implemented.

B.C	$\mathbf{v} = (v_1, v_2)$	$\mathbf{v} = (v_1, 0)$	$\mathbf{v} = (0, v_2)$
Navier-slip	36	22	25
Dirichlet	22	22	18

Table 6.1: Number of iterations for obtaining the convergence criteria of the CGM.

Table 6.2 and Figure 6.1 show the L^2 -norm of the velocity vector field for the null control problems as time function. The numerical control function \mathbf{v} has all possible structures, namely, $\mathbf{v} = \mathbf{0}$, $\mathbf{v} = (v_1, v_2)$, $\mathbf{v} = (v_1, 0)$ and $\mathbf{v} = (0, v_2)$.

On the other hand, for every possible structure of control mentioned above, Figure 6.2 and Figure 6.3 show cuts of the first and second component of the state $\mathbf{y} = (y_1, y_2)$ with the plane $x = 0.1$. Every figure displays a type of boundary condition. In order to appreciate a major difference in each case (due to scale), we decide to draw the slice at the time interval $[0.2, 0.25]$.

t	$\mathbf{v} = \mathbf{0}$	$\mathbf{v} = (v_1, v_2)$	$\mathbf{v} = (v_1, 0)$	$\mathbf{v} = (0, v_2)$	t	$\mathbf{v} = \mathbf{0}$	$\mathbf{v} = (v_1, v_2)$	$\mathbf{v} = (v_1, 0)$	$\mathbf{v} = (0, v_2)$
0.005	2.30E+00	2.30E+00	2.30E+00	2.30E+00	0.005	2.34E+00	2.20E+00	2.23E+00	2.22E+00
0.025	1.28E+00	1.27E+00	1.27E+00	1.27E+00	0.025	1.62E+00	1.19E+00	1.29E+00	1.28E+00
0.05	6.11E-01	6.08E-01	6.09E-01	6.09E-01	0.05	1.34E+00	8.22E-01	9.43E-01	9.50E-01
0.075	2.93E-01	2.89E-01	2.90E-01	2.90E-01	0.075	1.26E+00	6.89E-01	8.18E-01	8.33E-01
0.1	1.40E-01	1.37E-01	1.38E-01	1.38E-01	0.1	1.23E+00	5.93E-01	7.29E-01	7.49E-01
0.125	6.73E-02	6.36E-02	6.44E-02	6.44E-02	0.125	1.22E+00	5.02E-01	6.41E-01	6.65E-01
0.15	3.22E-02	2.87E-02	2.94E-02	2.94E-02	0.15	1.21E+00	4.14E-01	5.53E-01	5.78E-01
0.175	1.55E-02	1.20E-02	1.28E-02	1.28E-02	0.175	1.21E+00	3.29E-01	4.64E-01	4.88E-01
0.2	7.40E-03	4.37E-03	5.01E-03	5.01E-03	0.2	1.21E+00	2.46E-01	3.75E-01	3.97E-01
0.225	3.55E-03	1.18E-03	1.67E-03	1.67E-03	0.225	1.21E+00	1.61E-01	2.88E-01	3.06E-01
0.25	1.70E-03	2.18E-04	4.68E-04	4.66E-04	0.25	1.21E+00	9.63E-02	2.23E-01	2.36E-01

Table 6.2: L^2 -norm square of the solution of the null control problem with different internal controls. Dirichlet boundary condition (left) and Navier-slip boundary condition (right).

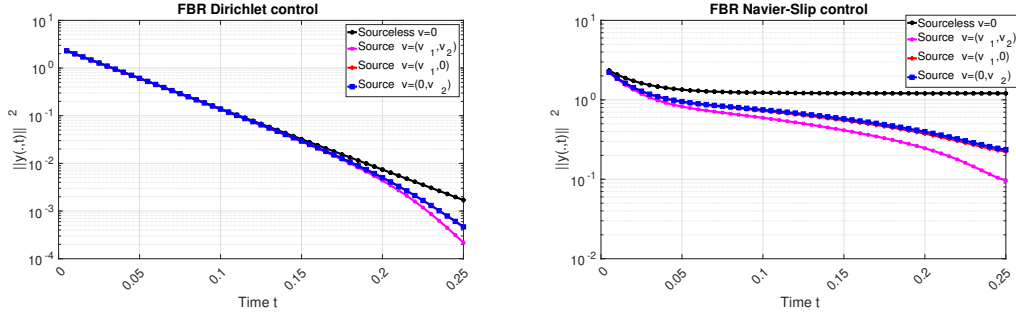


Figure 6.1: L^2 -norm square of the velocity field (as time function) of the solution of the null control problem with controls $\mathbf{v} = \mathbf{0}$ (black), $\mathbf{v} = (v_1, v_2)$ (pink), $\mathbf{v} = (v_1, 0)$ (red) and $\mathbf{v} = (0, v_2)$ (blue). Dirichlet boundary condition (left) and Navier-slip boundary condition (right).

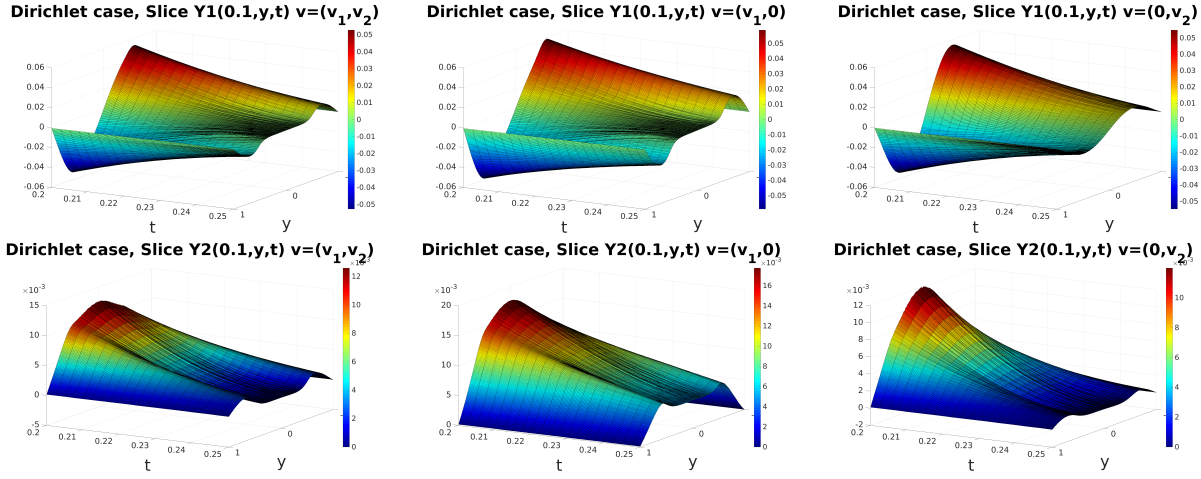


Figure 6.2: Dirichlet boundary conditions. Cut sections of the components of the state $\mathbf{y} = (y_1, y_2)$ by the plane $x = 0.1$. Cut section of y_1 (first row) and cut section of y_2 (second row). A different control function is represented in each column.

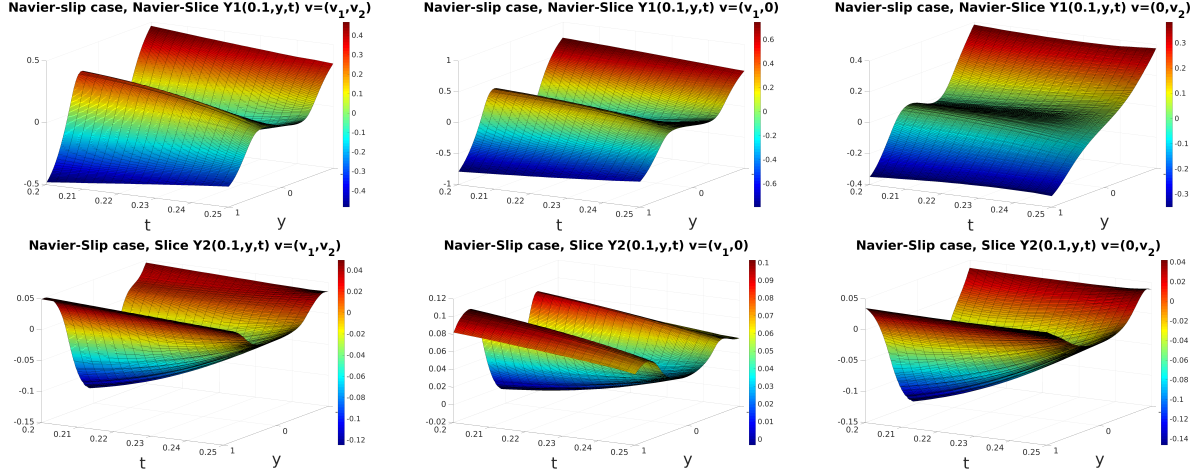


Figure 6.3: Navier–slip boundary conditions. Cut sections of the components of the state $\mathbf{y} = (y_1, y_2)$ by the plane $x = 0.1$. Cut section of y_1 (first row) and cut section of y_2 (second row). A different control function is represented in each column.

Remark 6.2. Observe that Figures 6.2, 6.3 allow us to visualize the impact of every boundary condition in the null control problem (2.1), that is, for every possible control function \mathbf{v} supported in the observatory $\omega = \{(x, y) \in \mathbb{R}^2 : x^2 + y^2 < 0.25\}$, even with one single scalar control, the system (2.1) with Dirichlet boundary conditions provides a faster solution in the sense that the L^2 –norm of the state goes to zero with a higher order than by considering homogeneous Navier–slip conditions. Numerically, this behaviour was described in Table 6.2, however, to understand the balance between Dirichlet and Navier–slip conditions and the convergence order of the state associated to the null control problem, it is interesting to consider friction between the fluid and the boundary (that is, nonhomogeneous Navier–slip conditions) as well as review the stability for the Stokes system with Navier–slip conditions [DLX18].

6.2 FEM

Taking as starting point the classical optimal control problem for the Stokes system [GLH08], we can solve the optimality system given in (2.1) (2.6) and (2.7) in a similar sense. Here, we only test the Dirichlet boundary conditions. In our case, the time–space discretization of the coupled system (2.1), (2.7) lies in a mixed finite element formulation in space using \mathcal{P}_2 –type elements for the velocity and \mathcal{P}_1 –type elements for the pressure, meanwhile finite differences are used for the time discretization (see [GP92, GR12, All05] for a complete review).

In this case, the number of iterations to achieve the stopping criteria $\epsilon = 10^{-8}$ in the CGM implemented is 17, for every control function (i.e., $\mathbf{v} = (v_1, v_2)$, $\mathbf{v} = (v_1, 0)$, $\mathbf{v} = (0, v_2)$). Table 6.4 and Figure 6.4 display the evolution in time of the L^2 –norm of the velocity vector field $\mathbf{y} = (y_1, y_2)$, which represents the solution to the null control problem (2.1), and where the control function v has different structure, namely, $\mathbf{v} = 0$, $\mathbf{v} = (v_1, v_2)$, $\mathbf{v} = (v_1, 0)$ and $\mathbf{v} = (0, v_2)$.

t	$\mathbf{v} = \mathbf{0}$	$\mathbf{v} = (v_1, v_2)$	$\mathbf{v} = (v_1, 0)$	$\mathbf{v} = (0, v_2)$
0.005	2.30E+00	2.30E+00	2.30E+00	2.30E+00
0.025	1.28E+00	1.27E+00	1.27E+00	1.27E+00
0.05	6.11E-01	6.08E-01	6.09E-01	6.09E-01
0.075	2.93E-01	2.89E-01	2.90E-01	2.90E-01
0.1	1.40E-01	1.37E-01	1.37E-01	1.37E-01
0.125	6.73E-02	6.36E-02	6.43E-02	6.43E-02
0.15	3.22E-02	2.86E-02	2.94E-02	2.94E-02
0.175	1.54E-02	1.20E-02	1.27E-02	1.27E-02
0.2	7.40E-03	4.32E-03	5.00E-03	5.00E-03
0.225	3.55E-03	1.17E-03	1.67E-03	1.67E-03
0.25	1.70E-03	2.29E-04	4.82E-04	4.82E-04

Table 6.3: Evolution in time of the L^2 -norm for the solution of the null control problem with Dirichlet boundary conditions and few scalar controls.

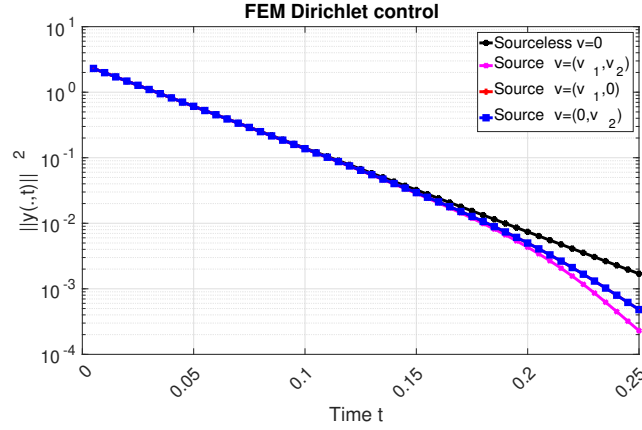


Figure 6.4: Evolution in time of the L^2 -norm square for the solution of the null control problem with Dirichlet boundary conditions and $v = 0$ (black), $v = (v_1, v_2)$ (pink), $v = (v_1, 0)$ (red) and $v = (0, v_2)$ (blue).

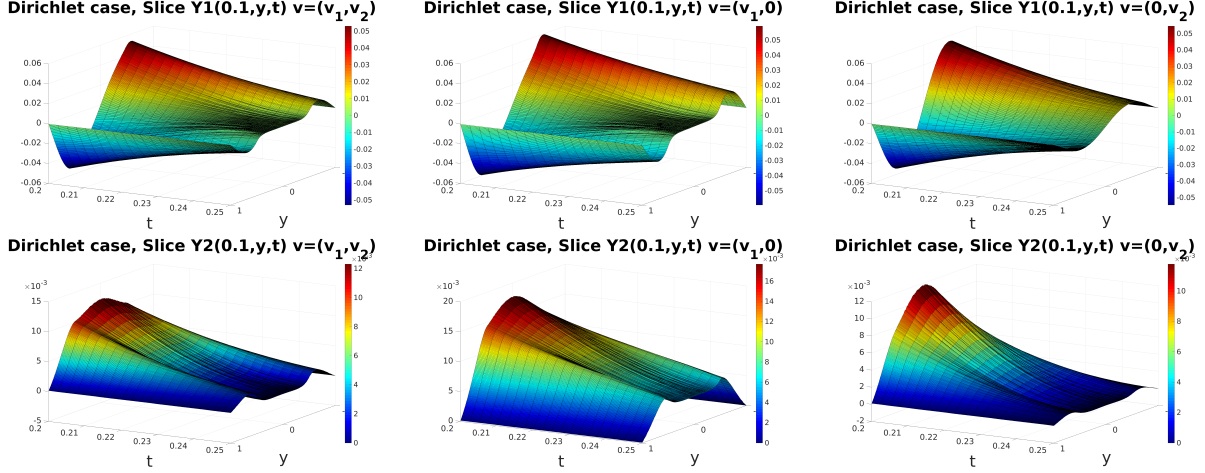


Figure 6.5: Dirichlet boundary conditions. Cut sections of the components of the state $\mathbf{y} = (y_1, y_2)$ by the plane $x = 0.1$. Cut section of y_1 (first row) and cut section of y_2 (second row). A different control function is represented in each column.

Remark 6.3. As we can see from Tables 6.3, 6.2 and Figures 6.5, 6.2 for the Dirichlet case, the control result using RBF-LHI or FEM are practically the same, but nevertheless RBF-LHI method has the advantage of being meshless and having more accuracy by using divergence free kernels.

Unfortunately, by observing the required number of iterations for the CGM in its convergence in both methods, RBF-LHI and FEM, the number is higher for the RBF-LHI method, this might be explained due that in RBF-LHI we are using \mathcal{P}_1 -type elements approximation to compute the integrals expressions in the CGM, meanwhile for FEM we are using \mathcal{P}_2 -type elements.

7 Conclusions and final remarks

In this article we have introduced a radial basis function, (RBFs), method to solve null control problems for the Stokes system with few internal scalar controls and Dirichlet or Navier-slip boundary conditions. As far as to our knowledge, this problem has not been treated in the literature through radial basis function methods. The continuous control problem gives rise to a coupled system of Stokes problems, namely the direct and adjoint systems. A conjugate gradient algorithm, adapted to the RBF setting is used to deal with this problem. Direct RBF solvers were designed, based on divergence free global vector RBF to avoid saddle point problems and thus inf/sup conditions. The pressure and the velocity are incorporated in the solution, in the sense of Wendland [Wen09], so that slip boundary conditions can be implemented. Within the paper, we formulate direct algorithms both for stationary and evolutionary Stokes systems. Stability analysis in the sense of Chinchapatnam [CDN06], that is by bounding the absolute value of the spectral radius of the discrete system, is performed for each of the techniques formulated within the article.

We note that recently, Keim and Wendland in [KW16] proposed a RBF compact support method for evolutionary Stokes problem with Dirichlet boundary conditions. This is an alternative methodology to the LHI-technique presented in this article.

It is worth pointing that when the stability condition was not satisfied the numerical solution was numerically ill posed.

The treatment of Navier-slip boundary conditions by the LHI method, which gave excellent results of order 10^{-4} in the L^∞ -norm, were obtained by incorporating the slip boundary oper-

ator in the ansatz. This was done without increasing the node density near the boundary or incorporating ghost nodes.

The LHI divergency free technique opens the possibility of treating a large number of data, whenever the fill distance and the shape parameter does not produces a singular value of the corresponding Gram matrix in extended precession. The use of extended precession to deal with the bad condition number has been formerly proposed by E. Kansa, [KH17] and S. Sarra, [Sar11], providing a good possibility to solve many real problems. However, we note that, recently, see Fronberg et al. [FF15] and references therein, have formulated several techniques to deal with the bad condition problem. These techniques will be the subject of further works to treat null control problems.

This paper opens the possibility of extending the stability analysis in order to obtain an explicit CLF type condition depending on the shape parameter, fill distance and the diffusion coefficient. Also, it may be possible to extend this analysis to the treatment of Navier–Stokes control problems. This will be considered in further works.

Acknowledgements. The research was partially supported by Fondecyt grant 3180100 (Cristhian Montoya). The authors acknowledge the CONACYT, project Fordecyt 265667. This work also was supported by the National Autonomous University of México [grant: PAPIIT, IN102116] and by Network of Mathematics and Development of CONACYT. We wish also to thanks Dr. Jesús López Estrada for providing some inside in development of the numerical code for this paper.

References

- [AB91] Luca Amodei and MN Benbourhim. A vector spline approximation. *Journal of approximation theory*, 67(1):51–79, 1991.
- [All05] Grégoire Allaire. *Analyse numérique et optimisation: une introduction à la modélisation mathématique et à la simulation numérique*. Editions Ecole Polytechnique, 2005.
- [BCM01] David L Brown, Ricardo Cortez, and Michael L Minion. Accurate projection methods for the incompressible navier–stokes equations. *Journal of computational physics*, 168(2):464–499, 2001.
- [CDN06] PP Chinchapatnam, K Djidjeli, and PB Nair. Unsymmetric and symmetric meshless schemes for the unsteady convection–diffusion equation. *Computer methods in applied mechanics and engineering*, 195(19-22):2432–2453, 2006.
- [Ceb12] Tuncer Cebeci. *Analysis of turbulent boundary layers*, volume 15. Elsevier, 2012.
- [CG13] Nicolás Carreno and Sergio Guerrero. Local null controllability of the n -dimensional navier–stokes system with $n-1$ scalar controls in an arbitrary control domain. *Journal of Mathematical Fluid Mechanics*, pages 1–15, 2013.
- [CGCG⁺13] D.A. Cervantes, P. González-Casanova, C. Gout, L.H. Juárez, and L.R. Reséndiz. Vector field approximation using radial basis functions. *Journal of Computational and Applied Mathematics*, 240:163 – 173, 2013.
- [CGCGM18] D.A. Cervantes, P. González-Casanova, C. Gout, and M.A. Moreles. A line search algorithm for wind field adjustment with incomplete data and rbf approximation. *Computational and Applied Mathematics*, 37(3):2519–2532, 2018.
- [CL14] Jean-Michel Coron and Pierre Lissy. Local null controllability of the three-dimensional navier–stokes system with a distributed control having two vanishing components. *Inventiones mathematicae*, 198(3):833–880, 2014.

- [Cor96] Jean-Michel Coron. On the controllability of the 2-d incompressible navier- stokes equations with the navier slip boundary conditions. *ESAIM: Control, Optimization and Calculus of Variations*, 1:35–75, 1996.
- [DLX18] Shijin Ding, Quanrong Li, and Zhouping Xin. Stability analysis for the incompressible navier–stokes equations with navier boundary conditions. *Journal of Mathematical Fluid Mechanics*, 20(2):603–629, 2018.
- [Fas07] Gregory E Fasshauer. *Meshfree Approximation Methods with Matlab:(With CD-ROM)*, volume 6. World Scientific Publishing Co Inc, 2007.
- [FCGIP04] Enrique Fernández-Cara, Sergio Guerrero, O Yu Imanuvilov, and J-P Puel. Local exact controllability of the navier–stokes system. *Journal de mathématiques pures et appliquées*, 83(12):1501–1542, 2004.
- [FCLdM15] Enrique Fernández-Cara, J Limaco, and SB de Menezes. Theoretical and numerical local null controllability of a ladyzhenskaya–smagorinsky model of turbulence. *Journal of Mathematical Fluid Mechanics*, 17(4):669–698, 2015.
- [FCMS17] Enrique Fernández-Cara, Arnaud Münch, and Diego A Souza. On the numerical controllability of the two-dimensional heat, stokes and navier–stokes equations. *Journal of Scientific Computing*, 70(2):819–858, 2017.
- [FF15] B. Fornberg and N. Flyer. *A primer on radial basis functions with applications to the geosciences*. Society for Industrial and Applied Mathematics, Philadelphia, PA, 2015.
- [FI96] Andrej Vladimirović Fursikov and O Yu Imanuvilov. *Controllability of evolution equations*. Number 34. Seoul National University, 1996.
- [FI99] Andrei Vladimirovich Fursikov and O Yu Imanuvilov. Exact controllability of the navier-stokes and boussinesq equations. *Russian Mathematical Surveys*, 54(3):565–618, 1999.
- [FLP13] B. Fornberg, E. Lehto, and C. Powell. Stable calculation of gaussian-based rbf-fd stencils. *Computers and Mathematics with Applications*, 65(4):627 – 637, 2013.
- [FSW16] Edward J Fuselier, Varun Shankar, and Grady B Wright. A high-order radial basis function (rbf) leray projection method for the solution of the incompressible unsteady stokes equations. *Computers & Fluids*, 128:41–52, 2016.
- [GL94] R Glowinski and JL Lions. Exact and approximate controllability for distributed parameter systems. *Acta numerica*, 1:269–378, 1994.
- [GLH08] Roland Glowinski, Jacques-Louis Lions, and Jiwen He. *Exact and Approximate Controllability for Distributed Parameter Systems: A Numerical Approach (Encyclopedia of Mathematics and its Applications)*. Cambridge University Press, 2008.
- [GM18] Sergio Guerrero and Cristhian Montoya. Local null controllability of the n-dimensional navier–stokes system with nonlinear navier-slip boundary conditions and n- 1 scalar controls. *Journal de Mathématiques Pures et Appliquées*, 113:37–69, 2018.
- [GMO17] Galina C García, Cristhian Montoya, and Axel Osses. A source reconstruction algorithm for the stokes system from incomplete velocity measurements. *Inverse Problems*, 33(10):105003, 2017.
- [GP92] Roland Glowinski and Olivier Pironneau. Finite element methods for navier-stokes equations. *Annual review of fluid mechanics*, 24(1):167–204, 1992.
- [GR12] Vivette Girault and Pierre-Arnaud Raviart. *Finite element methods for Navier-Stokes equations: theory and algorithms*, volume 5. Springer Science & Business Media, 2012.

- [Gue06] Sergio Guerrero. Local exact controllability to the trajectories of the navier-stokes system with nonlinear navier-slip boundary conditions. *ESAIM: Control, Optimisation and Calculus of Variations*, 12(3):484–544, 2006.
- [GZ18] P. González Casanova and J. Zavaleta. Radial basis function methods for optimal control of the convection-diffusion equation. *ArXiv e-prints*, March 2018.
- [HW09] Qiaolin He and X-P Wang. Numerical study of the effect of navier slip on the driven cavity flow. *ZAMM-Journal of Applied Mathematics and Mechanics/Zeitschrift für Angewandte Mathematik und Mechanik*, 89(10):857–868, 2009.
- [Ima97] Oleg Yu Imanuvilov. Local exact controllability for the 2-d navier-stokes equations with the navier slip boundary conditions. In *Turbulence Modeling and Vortex Dynamics*, pages 148–168. Springer, 1997.
- [KH17] E.J. Kansa and P. Holoborodko. On the ill-conditioned nature of c^∞ rbf strong collocation. *Engineering Analysis with Boundary Elements*, 78:26–30, 2017.
- [KW16] Christopher Keim and Holger Wendland. A high-order, analytically divergence-free approximation method for the time-dependent stokes problem. *SIAM J. Numerical Analysis*, 54:1288–1312, 2016.
- [Lam91] John Denholm Lambert. *Numerical methods for ordinary differential systems: the initial value problem*. John Wiley & Sons, Inc., 1991.
- [LSW17] E. Lehto, V. Shankar, and G-B. Wright. A radial basis function (RBF) compact finite difference (FD) scheme for reaction-diffusion equations on surfaces. *SIAM J. Scientific Computing*, 39(5), 2017.
- [Nav23] CLMH Navier. Mémoire sur les lois du mouvement des fluides. *Mem. Acad. Sci. Inst. Fr*, 6(1823):389–416, 1823.
- [NW94] Francis J Narcowich and Joseph D Ward. Generalized hermite interpolation via matrix-valued conditionally positive definite functions. *Mathematics of Computation*, 63(208):661–687, 1994.
- [Pea13] Pearson. A radial basis function method for solving pde-constrained optimization problems. *Numerical Algorithms*, 64:481–506, 2013.
- [Sar11] S.A. Sarra. Radial basis function approximation methods with extended precision floating point arithmetic. *Engineering Analysis with Boundary Elements*, 35(1):68–76, 2011.
- [SPLM11] D Stevens, H Power, M Lees, and H Morvan. A local hermitian rbf meshless numerical method for the solution of multi-zone problems. *Numerical Methods for Partial Differential Equations*, 27(5):1201–1230, 2011.
- [Wen04] Holger Wendland. *Scattered data approximation*, volume 17. Cambridge university press, 2004.
- [Wen09] Holger Wendland. Divergence-free kernel methods for approximating the stokes problem. *SIAM Journal on Numerical Analysis*, 47(4):3158–3179, 2009.